International Journal of Sciences: Basic and Applied Research (IJSBAR)

ISSN 2307-4531
(Print & Online)

https://gssrr.org/index.php/JournalOfBasicAndApplied/index

Natural Radioactivity Levels and Radiogenic Heat Production in River Sediments from Gulu and Amuru Districts, Northern Uganda

Amos Olanya[a*], Denis Okello[b], Bosco Oruru[c], Akisophel Kisolo[d]

[a,b,c,d] *Department of Physics, College of Natural Sciences, Makerere University, P.O Box 7062, Kampala, Uganda*

[a]*Email: olanyaamos38@gmail.com,* [b]*Email: dekello@mak.ac.ug,* [c]*Email: bosco.oruru@mak.ac.ug*

[d]*Email: akisolo@physics.mak.ac.ug*

Abstract

The activity concentrations (*AC*) of ^{238}U, ^{232}Th and ^{40}K in sediments from Gulu and Amuru districts, Uganda were determined using NaI(Tl) detector at Physics Department, Makerere University, Kampala to obtain; radioelement concentrations (*RC*), radiogenic heat production (*RHP*) and associated heat flow (H_f). The *AC* varied from (36.1 ± 2.3 - 261.2 ± 15.3) for ^{238}U, (97.4 ± 13.5 - 334.2 ± 36.6) for ^{232}Th, and (47.5 ± 3.9 - 1442.3 ± 58.9) Bq kg^{-1} for ^{40}K, with averages of 89.6 ± 6.3, 168.6 ± 17.9, and 275.4 ± 14.0 Bq kg^{-1}, respectively, above the world limits of 35, 30, and 400 Bq kg^{-1}, for ^{238}U, ^{232}Th and ^{40}K. The *RC* varied from (2.9 ± 0.2 - 20.8 ± 1.2) ppm for ^{238}U, (23.9 ± 3.3 - 82.0 ± 9.2) ppm for ^{232}Th, and (0.2 ± 0.01 - 3.2 ± 0.1) % for ^{40}K, with averages of 7.1 ± 0.5 ppm, 41.3 ± 4.3 ppm, and 1.1 ± 0.05%, respectively. The ^{238}U and ^{232}Th averages were above the Earth's crust values of 3 ppm and 12 ppm, respectively. The ^{40}K average is below the Earth's crust value of 2.33%. The *RHP* varied from (2.5 ± 0.6 - 10.2 ± 2.6) µW m^{-3} with an average of 4.5 ± 1.1 µW m^{-3}, above the world average of 4µW m^{-3}. High and moderate *RHP*, each account for 50% of the samples. The overall *RHP* mainly depended on ^{232}Th amounts, with 60% contribution. However, an increase in the *AC* of ^{238}U, ^{232}Th and ^{40}K reflected the integrated effect of *RHP*. The H_f varied from (19.6 ± 1.0 - 80.0 ± 4.0) mW m^{-2} with an average of 35.3 ± 1.8 mW m^{-2}. The high *RHP* and H_f values indicates feasibility for geothermal exploration. This calls for further studies to validate these findings.

Received: 7/11/2023
Accepted: 8/16/2023
Published: 8/28;/2023

---

* Corresponding author.

Keywords: Activity Concentrations; Radioelement Concentrations; Radiogenic Heat Production; Sediments.

1. Introduction

The natural radioactivity levels are useful in delineating the health effects of prolonged exposure to the source on human, animal and the environment [1, 2, 3]. The natural radioactivity of significance in this study are ^{238}U, ^{232}Th and ^{40}K [4, 5]. These isotopes have half-lives comparable to the age of the Earth (about 10^{10} years) and are still extant as significant heat sources in the Earth's crust [6, 7, 41:243]. The ^{238}U, ^{232}Th and ^{40}K have average abundances of about 3 ppm, 12 ppm, and 120 ppm in the Earth's crust [8, 9]. The decay of ^{238}U, ^{232}Th and ^{40}K in the Earth's crust emits energetic particles (α-particles, and β-particles) and γ-rays. Except for the energy taken by the neutrino, the whole decay is converted to heat [10]. The reactions are as illustrated in Equations (1) – (4).

$$^{238}_{92}U \rightarrow {}^{206}_{82}Pb + 8^{4}_{2}H_e + 6e + 6anti - v + 51.667\ MeV, (1)$$

$$^{232}_{90}Th \rightarrow {}^{208}_{82}Pb + 6^{4}_{2}H_e + 4e + 4anti - + 42.793 MeV, (2)$$

$$^{40}_{19}K \rightarrow {}^{40}_{20}C_a + anti - v + e + 1.321\ MeV\ (89\%), (3)$$

$$^{40}_{19}K + e \rightarrow {}^{40}_{18}Ar + v + 1.513\ MeV\ (11\%), (4)$$

The decay of ^{238}U and ^{232}Th are the prevalent heat producers today with heat production constants of 9.52 x 10^{-5} w kg^{-1} and 2.56 x 10^{-5} w kg^{-1}, respectively [11]. The ^{40}K is the least heat producer compared to ^{238}U, and ^{232}Th with heat production constant of 3.48 x 10^{-9} w kg^{-1}[12]. The heat produced in the mantle and crust of the Earth during the decay of ^{238}U, ^{232}Th and ^{40}K is importantly called the Radiogenic Heat Production or *RHP* [9,13]. The *RHP* determines the heat flow in the basement rocks from which river sediments are formed and has been used for the assessment of geothermal resources in many parts of the world [14, 15]. River sediments pile and transfer contaminant within the geographic region and is considered the environmental host of the waste discharged by natural or man-made processes in our surroundings [6, 16, 17]. Most river sediments are formed when the rock and organic materials are broken into small pieces by fluvial means which enhance the levels of natural radioactivity in river sediments [17, 18]. The *RHP* is influenced by the sediments' lithological and geochemical features as reported by [9, 19]. Natural radioactivity has been intensively studied [12, 15, 17, 20]. Sathish *and colleagues* [12] recently assessed the natural radiation hazards and function of heat production rate in lake sediments, India using NaI(Tl) detector. The study attributed the radioactive heat production ranges of 0.06 - 0.23 µW m^{-3} to the high concentration and density of radioactive minerals in the lake sediments. In determination of natural radioactivity concentration and radiogenic heat production in selected quarries in Ondo State, Nigeria, by Gamma Surveyor, Asere *and colleagues* [15] reported total heat production and heat flow ranges of 0.97 – 5.3 µW m^{-3} and 7.63 – 42.12 mW m^{-2}, respectively. The study recommended further probe for potential geothermal exploration. In 2018, Ghania, Fatima & Mourad [17] determined the levels and effects of natural radionuclides in sediment banks of Rhumel River (Northeast Algeria) using high resolution HPGe detector. Results of this study shows that the mean *AC* were; 26.64 Bq Kg^{-1} for ^{226}Ra, 25.95 Bq Kg^{-1} for ^{232}Th and 164.50 Bq Kg^{-1} for ^{40}K. The variations in the *AC* were attributed to inhomogeneous samples composition.

Natural radioactivity levels and associated radiation hazards in Nile river sediments, Egypt were also investigated using NaI(Tl) detector by El-Taher & Adel [16]. The higher concentrations of the radionuclides were attributed to industrial wastes. Biira, Kisolo & D'ujanga [20] determined the concentration levels of radon in Tororo and Busia districts, Eastern Uganda using activated charcoal canisters and NaI(Tl) detector. It was found that the mean radon concentrations values were below the United Nations Scientific Committee on the Effect of Atomic Radiation (*UNSCEAR*) and International Commission of Radiological Protection (*ICRP*) recommended radon action level of 200 Bq m^{-3}. Similar assessments for the dormitories of secondary schools in Otuke district, Uganda based on survey meters and activated charcoal canister were made by Oruru, Todo & Kisolo [10]. The measured radon concentrations were below the World Health Organization (*WHO*) action level of 100 Bq m^{-3}. A study by [33] in selected quarries in Northern Uganda using NaI(Tl) detector, reported the average *AC* as: 57.1 ± 4.7 for ^{238}U, 122.3 ± 11.1 for ^{232}Th, and 914.2 ± 30.3 Bq kg^{-1} for ^{40}K, well above the global limits. It was concluded that the workers and inhabitant were exposed to significant background radiations from quarries. The determination of *RHP* in river sediments for the assessment of geothermal resources in the districts of Gulu and Amuru, Uganda have not yet been done, but very significant. A study by Ojara & Odongkara [21] reported the needs to develop geothermal energy as an alternative energy source to hydro and others to meet the energy demand of the locals.

This paper, therefore, reports the results of: (i) the *AC* of ^{238}U, ^{232}Th and ^{40}K; (ii) the *RC* of ^{238}U, ^{232}Th and ^{40}K; (iii) the *RHP* and (iv) H_f in 30 representative sediment samples from Gulu and Amuru districts, Northern Uganda, in order to estimate the area's geothermal potential. The results of this study may be used by Uganda Geological Survey and Mines (*UGSM*) for geothermal exploration and eventual development of geothermal energy project. Also, Gulu and Amuru districts could use these findings to raise awareness on the viable local geothermal sources and support its development as a proxy for energy source. However, this study did not consider the energies produced by α and β particles which are significant radiation dose to lungs and other respiratory organs.

1.1. Description and Geology of Study Area

This study was conducted in the districts of Gulu ($2^{o}10'$ and $03^{o}6'$ N, $32^{o}10'$ and $33^{o}30'$ E) and Amuru ($2^{o}35'$ and $03^{o}45'$ N, $31^{o}30'$ and $32^{o}10'$ E) in Northern Uganda, illustrated in Figure 1 and Table 1, respectively. The districts were chosen due to the rapid growth in agriculture, commerce, tourism, industry and lucrative trade links with South Sudan. The selected areas had total population of 187,124 persons (constituting 30% of the population of the two districts). The relief consists of complex low landscape with relatively uniform topography and altitude ranging from 775 - 1106 m above sea level. The temperature varied from (18 – 30) ^{0}C [21]. The unit is mainly composed of Neoarchean gneissose-migmatic rocks and granitoids with the quartzo-feldspathic veins cut by colored layers of granite rich in Quartz (SiO_2), plagioclase ($NaAlSi_3O_8$), feldspar ($KAlSi_3O_8$), iron oxide (Fe_2O_3), opaque minerals, biotite K $(Mg, Fe^{+2})_3(Al, Fe^{+3})\ Si_3O_{10}(OH, F)_2$, and muscovite $KAl_2(AlSi_3)\ O_{10}(OH)_2$ [22]. Due to the up and down wrapping of the basement rocks consisting of uniform rock structure, the drainage pattern formed network of rivers which drain their waters into Albert Nile, Victoria Nile and Achwa River at acute angles [21]. The network of rivers is analogous to branches of trees and formed V-shaped patterns. The said rivers offer immense environmental and socio economic values and services to the

population such as: crop farming, brick-laying, pottery, sand mining, irrigation development, commercial tree seedlings, horticulture and fish farming. The rivers traversing the two districts include among others: Unyama, Ayugi, Omee, Aswa, Tangi, Ayago, Oitino, Abera, Ziola, Awicpalaro, and Tochi. The reader is referred to illustration in Figure 1 for further details.

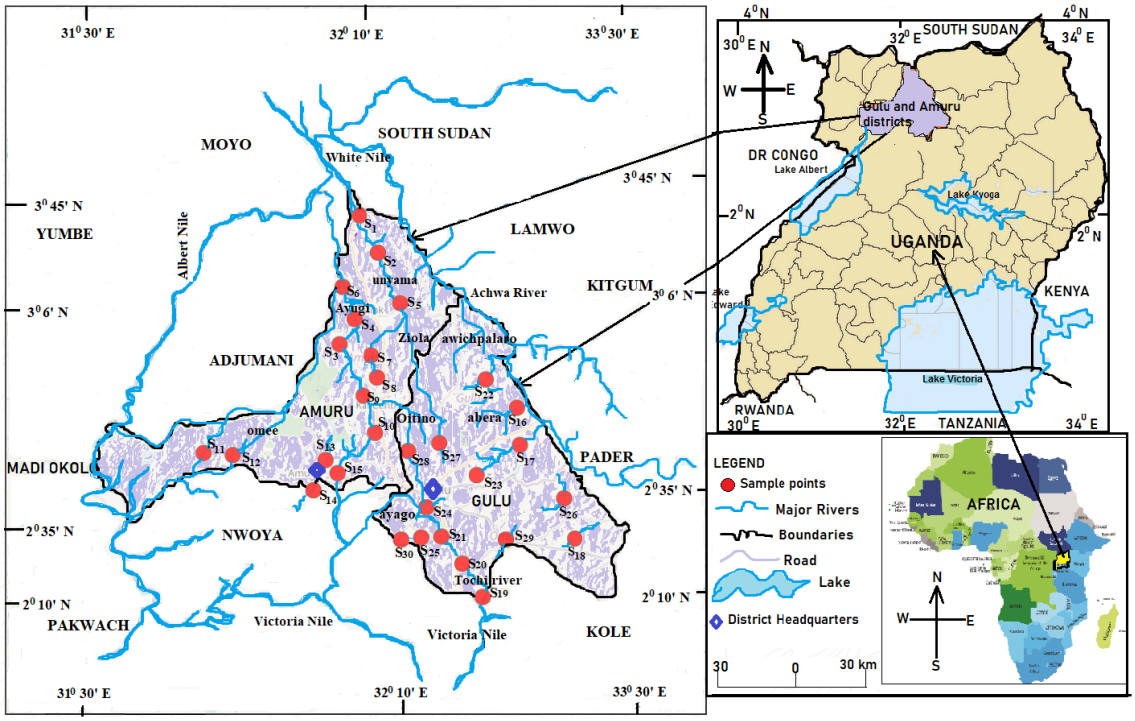

Figure 1: Map of Gulu and Amuru districts showing selected rivers and sample locations [23].

2. Materials and Methods

2.1 Sample Collection and Preparation

The sample locations, as in Table 1 and Figure 1, were identified from the Nile river major tributaries in Gulu and Amuru districts, 30 km apart in which river sand were mined, highly populated, and representative enough of the major river sediments types in the area. Different rivers dissecting heterogeneous geological settings were chosen to obtain representative number of sediment samples with various physical, chemical and geochemical behaviors to better understand the distribution pattern of ^{238}U, ^{232}Th and ^{40}K in the sediment samples as stated by Laith *and colleagues* [9]. At each site, a sample point from near the river bank of 10 – 100 cm was carefully selected where the survey meters indicated high dose rate as pointed in the study by Keser *and colleagues* [8], Oruru, Todo & Kisolo [10], and Atibu *and colleagues* [24]. The distance of 10 – 100 cm from the river bank was used so that samples could be taken from undisturbed area (closed system).

This was to limit the factors that could obscure the experimental outcome. Coordinates were recorded by high sensitivity (etrex) Garmin Global Position Satellite (*GPS*). A more complete details of the sampling sites and GPS coordinates can be found in Table 1.

Table 1: Sampling site and *GPS* coordinates of the sampled rivers in Gulu and Amuru district.

Site	*GPS* Coordinate			Elevation	Population
ID	Latitude	Longitude	Sampling Site	(*m*)	(*persons*)
S_1	30 30' 53.2506" N	320 5' 13.002" E	Bibia	980	7,934
S_2	30 24' 53.0094" N	320 8' 30.7536" E	Pacilo	775	4,143
S_3	30 19' 15.6864" N	320 2' 29.5146" E	Pogo	783	5,968
S_4	30 14' 1.5174" N	320 4' 33.4482" E	Palukere	808	2,633
S_5	30 16' 35.8458" N	320 12' 1.7598" E	Okidi	811	3,515
S_6	30 9' 49.7766" N	320 2' 0.1896" E	Pogo	783	5,968
S_7	30 8' 6.1116" N	320 7' 11.6538" E	Parubanga	1010	6,696
S_8	30 4' 28.689" N	320 8' 12.9876" E	Parubanga	903	6,696
S_9	30 1' 31.1766" N	320 5' 52.5516" E	Kal	953	4,980
S_{10}	20 55' 25.824" N	320 7' 51.204" E	Coke	1036	4,151
S_{11}	20 52' 25.1326" N	310 39' 40.4064" E	Pailyec	1073	15,042
S_{12}	20 51' 43.6356" N	310 44' 22.2072" E	Pailyec	1039	15,042
S_{13}	20 50' 59.193" N	310 59' 46.7052" E	Toro	1090	5,664
S_{14}	20 46' 2.9208" N	310 57' 48.0522" E	Paminrut	783	9,194
S_{15}	20 48' 50.8104" N	320 1' 35.4714" E	Pamuca	1049	5,383
S_{16}	20 59' 32.7336" N	320 31' 18.2598" E	Paibona	972	5,480
S_{17}	20 53' 27.3222" N	320 31' 49.8648" E	Kal Alii	1006	6,614
S_{18}	20 38' 10.6836" N	320 40' 49.1874" E	Lukwor	1052	6,390
S_{19}	20 28' 32.9484" N	320 25' 47.6112" E	Patek	1062	4,835
S_{20}	20 33' 59.691" N	320 22' 19.6428" E	Paidwe	1071	8,663
S_{21}	20 38' 28.7622" N	320 18' 49.4244" E	Labwoc	1090	5,676
S_{22}	30 4' 9.1554" N	320 26' 13.6824" E	Owalo	998	6,189
S_{23}	20 53' 47.0754" N	320 18' 28.9584" E	Oding	1043	3,524
S_{24}	20 38' 18.7152" N	320 15' 30.9816" E	Kal	1106	5,658
S_{25}	20 43' 17.835" N	320 16' 17.8422" E	Abwoc	1083	3,929
S_{26}	20 44' 44.235" N	320 39' 9.7374" E	Binya	1017	10,122
S_{27}	20 48' 31.0608" N	320 24' 44.694" E	Anyaya	1081	4,009
S_{28}	20 52' 28.0734" N	320 13' 22.44" E	Pabwo	1031	3,458
S_{29}	20 37' 58.962" N	320 29' 31.4334" E	Parwech	1005	4,384
S_{30}	20 37' 58.962" N	320 12' 13.2258" E	Onyona	1097	5,184

A sample of about 1 kg wet weight was then manually collected from each site at a depth of 5 – 10 cm from the river bed using a hand shovel within a sampling area of 1 m^2 [5, 7, 18, 25, 26]. The 1 kg sample was then put into a polyethene bag, sealed, and labeled with a file name to avoid cross contamination until analyzed [9]. The process was repeated for all the selected rivers until thirty (30) representative sediment samples were obtained. Stones and organic materials were removed from the sediment samples and then oven dried to 120 ^{0}C for nine hours until constant weight was attained [28]. This was done to ensure that moisture was completely removed from the sample in order to avoid clamping of the sample particles during crushing [6, 16, 29]. The sample was then grounded in a mortar using a pestle to powder form in order to increase the surface area and sieved through a 200 µm mesh sieve to homogenize the contents [4, 17, 30]. The sieved sample was then filled in air tight standard 500 ml plastic Marinelli beaker (to minimise radon leakage); labeled with a file name and weighed using a digital meter to determine the dry mass. The digital meter registered an average of 570 ± 0.1 g for each prepared samples [31, 32]. The air tight sealed sample was stored for four weeks (30 days), approximately 7 times the half-lives of the daughter nuclide before counting to obtain secular equilibrium between ^{226}Ra and decay products of ^{222}Rn (^{214}Pb & ^{214}Bi) [1, 2, 6, 33]. All the samples were then analyzed to show the geologic attributes of the study area.

2.2 Sample Analysis

2.2.1 Detector System and Calibration

The gamma ray detector used in this study is a Gammadata Matteknik (*GDM*) 20 Teledye NaI Iodide model, (version 1.2, 1997). The NaI(Tl) is the most widely used detector because it is the most efficient inorganic scintillator, cheap and readily available. The detector unit has a height of 94 cm, diameter 42 cm and weighs 350 kg. It has a 3 x 3 – inch active area with 14-pin Photo Multiplier Tube (*PMT*). It offers an energy resolution of < 7% Full Width at Half Maximum (*FWHM*) at the 662 keV ^{137}Cs line with cylindrical lead shielding of 10 cm thick and removal pellets of 315 kg. The detector unit consists of a high voltage supply *D*234 of 0 – 1500 V which is connected to a power source of ±15V, 500 mA. The whole system is connected to a computer interface, *IBM* computer-*IAEA*16867 (SS01/005), which has an inbuilt auto*DAS* software, (version 3.16). The energy and efficiency calibrations of the detector were done by common radioactive ^{152}Eu standard source from Gammadata Matteknik AB, Sweden (model number 26-Jan-1993 Europium-152). The source weighs 54 g with activity of 1370 ± 80 Bq and half-life of 3.2 years. The ^{152}Eu is a frequently used calibration source due to its wide range of gamma energies from 122 keV to 1460.8 keV [8, 9]. A spectrum for ^{152}Eu was collected for 5000 seconds and saved in the computer hard disc [20]. The peaks of known energies were analyzed for energy and efficiency calibrations. The energy resolution of the detector was also determined and found to be 6.2% at 662 keV. The background of the laboratory environment was determined by placing an empty Marinelli beaker on the detector with the same period and operating voltage used to determine the energy spectra of the samples [20, 32]. The background spectrum was later subtracted from the gamma ray spectra of the samples to obtain the net counts.

2.2.2 Activity Concentrations of ^{238}U, ^{232}Th and ^{40}K

When the analyzed sediment sample attained a state of secular equilibrium between ^{238}U and ^{232}Th with their progenies [18], the activity concentration (*AC*) of ^{238}U in the samples was obtained from the average energies of 351.9 keV of ^{214}Pb, and 609.3 keV of ^{214}Bi, respectively. Similarly, the *AC* of ^{232}Th was obtained from the average energies of 238.6 keV of ^{212}Pb, and 583.2 keV of ^{208}Tl, respectively [20, 34]. The *AC* of ^{40}K was determined directly from its 1460.8 keV gamma-ray peaks following the decay of ^{40}K [35]. Spectra peaks were analyzed one at a time using auto*DAS* command, whereby the cross was placed immediately at the left edge of the peak and *L* was typed to define the cross of the lower mark. The cross of the upper mark was similarly placed at the right edge of the same peak using command *U*. This was followed by typing *CEN* command which gave centroid, standard deviation, *FWHM*, sum between markers and rate [20, 33]. The *AC* of i^{th} nuclides from the respective energy peak was computed using the Equation (5) as stated by the authors in [9, 33, 36]:

$$AC_i(Bq\ kg^{-1}) = \frac{N_e}{M_i T \varepsilon \rho}, (5)$$

where $AC_i =$ Activity concentrations $(Bqkg^{-1})$ in the i^{th} sample. $N_e =$ net peak area of energy , e, (Bq). $M_i =$ dry mass of the i^{th} sample (kg). $T =$ the sample measurement time (seconds). $\varepsilon =$efficiency of the detector (%). $\rho =$ branching ratio (absolute gamma emission probability) (%).

2.3 Radioelement Concentrations (RC)

The *RC*, in parts per million (ppm) of ^{238}U, and ^{232}Th, and in (%) of ^{40}K in the sediment samples were numerically deduced from their measured *AC* values by the use of the Equations (6), (7) and (8) reported by [36, 37, 38], as;

$$U(ppm) = \left(\frac{C_U M_U}{N_A In2}\right) t_{1/2}\,, (6)$$

$$Th\ (ppm) = \left(\frac{C_{Th} M_{Th}}{N_A In2}\right) t_{1/2}, (7)$$

$$K(\%) = \left(\frac{C_K M_K}{N_A In2}\right) t_{1/2}, (8)$$

where: C_U, C_{Th}, and C_K are activity concentrations of ^{238}U, ^{232}Th and ^{40}K, respectively in Bq g^{-1}, M_U, M_{Th}, and M_K are molecular weights of ^{238}U, ^{232}Th and ^{40}K, respectively in g mol.$^{-1}$, N_A is Avogadro's number (6.02 x 10^{23}) and $t_{1/2}$ is the half-life of each of the natural radionuclides expressed in seconds as reported by Okeyode [39].

2.4 The Radiogenic Heat Production (RHP)

The *RHP* defines the amount of heat liberated in a unit time per unit volume of sediment by the decay of unstable radioactive isotopes; in unit of μW m^{-3}. The *RHP* is high in the upper crust and always low at the mantle reaching 1 – 2 μW m^{-3}. Murugesan *and colleagues* [13], and Okeyode [39] noted that high *RHP* are targets for geothermal exploration and production. The *RHP* in the studied samples was determined by Equation (9) as proposed by Rybach [19]. It should be appreciated that this model has been widely used and accepted beyond question by various scholars, including among others Sokari *and colleagues* [36], Omosule & Adelowo [38], and Murugesan *and colleagues* [40].

$$RHP\ (\mu W m^{-3}) = \beta\rho(f_U C_U + f_{Th} C_{Th} + f_K C_K), (9)$$

where: β is constant (10^{-5}), ρ is the average samples density (kg m^{-3}), C_U, and C_{Th} are ^{238}U and ^{232}Th concentrations (weight *ppm*), and C_K is the total ^{40}K concentrations (weight %). The numerical constants f_U, f_{Th}, and f_K used in the conversion were obtained by Rybach [19] and later on used in the study by Sokari *and colleagues* [36]. The constant for ^{238}U (9.52) is more than double the constants for ^{232}Th (2.56) and ^{40}K (3.48), reflecting the significant role that uranium has in producing heat compared with thorium or potassium [9]. The amount of heat that flows per second across a square meter of surface (H_f) was calculated using Equation (10) as introduced by Turcotte & Schubert [41] and later used for river sediment samples by Asere *and colleagues* [15] as;

$$H_f = -k\frac{dT}{dz} = \frac{RHP}{A}(M), (10)$$

where H_f is the heat flow in (mW m^{-2}), k is thermal conductivity ($Wm^{-1}K^{-1}$) , $\frac{dT}{dz}$ is geothermal gradient (K km^{-1}) M is the mass of the mantle plus crust (4.0 x 10^{24} kg), and A is the Earth's surface area (5.1 x 10^{8} km^2). On the basis of geochemical studies, the core can't contain a significant fraction of the heat-producing elements. Hence, the mass of the mantle is used instead of the Earth. According to Turcotte & Schubert [41], the mean H_f for all continents is 65 ± 1.6 mW m^{-2} with 37 mW m^{-2} as the fraction attributed to the decay of ^{238}U, ^{232}Th and ^{40}K. The remaining 28 mW m^{-2} was attributed to basal heating of the continental lithosphere by mantle convection. Determination of heat flow by Fourier's law ($-k\frac{dT}{dz}$) is beyond the scope of this work which requires further studies. The negative sign is needed to account for the direction of the heat flow; if temperature increases in the downward direction of the z-axis, the flow of heat from high to low temperature is upward.

3. Results

Table 2: The *AC, RC* and *RHP* of ^{238}U, ^{232}Th and ^{40}K in the sediment samples.

ID	^{238}U (*Bq kg^{-1}*)	^{232}Th (*Bq kg^{-1}*)	^{40}K (*Bq kg^{-1}*)	^{238}U (*ppm*)	^{232}Th (*ppm*)	Th/U	^{40}K (*%*)	*RHP*($\mu W\ m^{-3}$)
S_1	68.3 (5.6)	130.0 (27.6)	287.0 (12.3)	5.4 (0.5)	32.0 (3.8)	5.93	1.1 (0.04)	3.5 (0.9)
S_2	73.0 (5.7)	155.3 (15.9)	106.8 (10.0)	5.8 (0.5)	38.1 (3.9)	6.57	0.4 (0.03)	3.9 (1.0)
S_3	133.8 (13.8)	253.6 (27.4)	187.6 (6.2)	10.7 (1.1)	62.2 (6.9)	5.81	0.7 (0.02)	6.7 (1.7)
S_4	77.6 (6.6)	169.7 (18.1)	135.7 (8.0)	6.2 (0.5)	41.6 (4.5)	6.71	0.5 (0.03)	4.2 (1.1)
S_5	63.7 (5.9)	135.2 (19.5)	169.6 (9.1)	5.1 (0.5)	33.3 (4.8)	6.53	0.6 (0.03)	3.4 (0.9)
S_6	148.9 (5.6)	334.2 (36.6)	1442.3 (58.9)	11.9 (0.5)	82.0 (9.2)	6.90	5.5 (0.20)	8.6 (2.2)
S_7	63.9 (5.4)	138.9 (20.0)	189.9 (8.6)	5.1 (0.4)	34.1 (4.9)	6.69	0.7 (0.03)	3.5 (0.9)
S_8	88.5 (6.3)	154.5 (16.7)	247.9 (14.9)	7.0 (0.5)	36.8 (4.1)	5.26	0.9 (0.05)	4.2 (1.1)
S_9	77.9 (5.5)	132.0 (20.1)	284.9 (14.4)	6.2 (0.4)	32.4 (4.9)	5.23	1.1 (0.05)	3.7 (0.9)
S_{10}	75.0 (6.0)	124.2 (15.8)	575.0 (26.2)	6.0 (0.5)	30.5 (3.9)	5.08	2.2 (0.08)	3.5 (0.9)
S_{11}	36.1 (2.3)	151.1 (3.7)	222.2 (13.7)	2.9 (0.2)	37.1 (0.9)	12.80	0.8 (0.04)	3.1 (0.8)
S_{12}	156.2 (7.2)	288.0 (9.7)	339.9 (21.4)	12.4 (0.6)	70.6 (2.4)	5.69	1.3 (0.07)	7.6 (1.9)
S_{13}	101.7 (6.0)	181.5 (13.3)	234.0 (6.3)	8.1 (0.5)	44.5 (3.3)	5.49	0.9 (0.02)	5.0 (1.3)
S_{14}	261.2 (15.3)	319.5 (16.8)	218.2 (14.5)	20.8 (1.2)	78.4 (4.1)	3.77	0.8 (0.05)	10.2 (2.6)
S_{15}	64.7 (5.8)	128.0 (15.1)	105.2 (6.8)	5.1 (0.5)	31.4 (3.7)	6.16	0.4 (0.02)	3.2 (0.8)
S_{16}	78.6 (6.2)	114.6 (21.3)	164.8 (8.1)	6.3 (0.5)	28.1 (5.2)	4.46	0.6 (0.03)	3.4 (0.9)
S_{17}	83.7 (7.0)	162.5 (16.4)	295.9 (10.8)	6.7 (0.6)	39.9 (4.0)	5.96	1.1 (0.03)	4.3 (1.1)
S_{18}	43.5 (2.5)	101.1 (14.2)	172.8 (12.4)	3.5 (0.2)	24.8 (3.5)	7.09	0.7 (0.04)	2.5 (0.6)
S_{19}	88.3 (6.1)	161.2 (20.1)	201.5 (9.2)	7.0 (0.5)	39.5 (5.0)	5.64	0.8 (0.03)	4.4 (1.1)
S_{20}	99.9 (6.6)	195.0 (11.9)	105.5 (5.7)	8.0 (0.5)	47.8 (2.9)	5.98	0.4 (0.02)	5.0 (1.3)
S_{21}	112.3 (4.8)	198.0 (19.6)	188.5 (7.5)	8.9 (0.4)	48.6 (4.8)	5.46	0.7 (0.02)	5.4 (1.4)
S_{22}	72.7 (5.0)	134.7 (12.0)	213.7 (15.2)	5.8 (0.4)	33.0 (3.0)	5.69	0.8 (0.05)	3.6 (0.9)
S_{23}	67.0 (5.3)	134.2 (19.4)	370.4 (22.3)	5.3 (0.4)	32.9 (4.8)	6.21	1.4 (0.07)	3.5 (0.9)
S_{24}	86.7 (4.9)	164.4 (26.0)	829.1 (39.7)	6.9 (0.8)	40.3 (6.4)	5.84	3.2 (0 .10)	4.5 (1.1)
S_{25}	61.4 (5.7)	115.8 (19.7)	185.5 (11.5)	4.9 (0.5)	28.4 (4.8)	5.80	0.7 (0.04)	3.1 (0.8)
S_{26}	47.1 (6.3)	97.4 (13.5)	169.6 (9.1)	3.8 (0.5)	23.9 (3.3)	6.29	0.6 (0.03)	2.5 (0.6)
S_{27}	54.8 (5.5)	108.2 (18.8)	190.7 (9.6)	4.4 (0.4)	26.5 (4.6)	6.02	0.7 (0.03)	2.9 (0.7)
S_{28}	92.9 (6.9)	161.4 (15.7)	47.5 (3.9)	7.4 (0.6)	39.6 (3.9)	5.35	0.2 (0.01)	4.4 (1.1)
S_{29}	120.0 (5.8)	228.5 (16.9)	217.3 (11.5)	9.6 (0.5)	56.0 (4.2)	5.83	0.8 (0.04)	6.0 (1.5)
S_{30}	88.6 (5.8)	186.5 (15.4)	162.4 (11.2)	7.1 (0.5)	45.7 (3.8)	6.44	0.6 (0.04)	4.8 (1.2)
Ave	**89.6 (6.3)**	**168.6 (17.9)**	**275.4 (14.0)**	**7.1 (0.5)**	**41.3 (4.3)**	**6.09**	**1.1 (0.05)**	**4.5 (1.1)**
Mi.	**36.1 (2.3)**	**97.4 (13.5)**	**47.5 (3.9)**	**2.9 (0.2)**	**23.9 (3.3)**	**3.77**	**0.2 (0.01)**	**2.5 (0.6)**
Ma.	**261.2 (15.3)**	**334.2 (36.6)**	**1442.3 (58.9)**	**20.8 (1.2)**	**82.0 (9.2)**	**12.80**	**5.5 (0.20)**	**10.2 (2.6)**

Where: **Ave** is average; **Mi**. is minimum; **Ma**. is maximum.

The *AC, RC and RHP* of ^{238}U, ^{232}Th and ^{40}K in the experimentally analyzed samples were computed using

Equations (5) to (9) and are given in Table 2. The results show that ^{238}U, ^{232}Th and ^{40}K were the only radionuclides detected in all the samples but with uneven occurrences. As shown in Table 2, the *AC* varied from (36.1 ± 2.3 - 261.2 ± 15.3) Bq kg^{-1} for ^{238}U, (97.4 ± 13.5 - 334.2 ± 36.6) Bq kg^{-1} for ^{232}Th, and (47.5 ± 3.9 - 1442.3 ± 58.9) Bq kg^{-1} for ^{40}K, with averages of 89.6 ± 6.3, 168.6 ± 17.9, and 275.4 ± 14.0 Bq kg^{-1}, respectively. Figure 2 shows bar graphs of the *AC* of ^{238}U, ^{232}Th and ^{40}K in the samples. The data shows that the *AC* of ^{238}U is higher than that of ^{40}K in samples S_{14} and S_{28}. Also, the *AC* of ^{232}Th is highest in samples S_2, S_3, S_{14}, S_{15}, S_{20}, S_{21}, S_{28}, S_{29}, and S_{30} compared to ^{238}U, and ^{40}K. In 70% of the samples, the *AC* were in the order ^{40}K > ^{232}Th > ^{238}U. The *AC* of ^{238}U, ^{232}Th and ^{40}K in sample S_6 were significantly higher than the global averages of 35, 30, and 400 Bq kg^{-1} by factors of 4.3, 11.1, and 3.6, for ^{238}U, ^{232}Th and ^{40}K, respectively. The samples S_{10} (575.0 Bq kg^{-1}), and S_{24} (829.1 Bq kg^{-1}) had *AC* of ^{40}K higher than world average value of 400 Bq kg^{-1} by factors of 1.44 and 2.07, respectively. It is seen that 90% of the samples had *AC* of ^{40}K lower than world average value of 400 Bq kg^{-1}.

As illustrated in Table 2, The *RC* of ^{238}U, ^{232}Th and ^{40}K varied from (2.9 ± 0.2 - 20.8 ± 1.2) ppm, (23.9 ± 3.3 - 82.0 ± 9.2) ppm, and (0.2 ± 0.01 - 3.2 ± 0.1) %, with averages of 7.1 ± 0.5 ppm, 41.3 ± 4.3 ppm, and 1.1 ± 0.05% for ^{238}U, ^{232}Th and ^{40}K, respectively. The ranges for ^{238}U and ^{232}Th obtained in this study are above the normal continental crust ranges of 2 - 3 ppm, and 8 – 12 ppm, respectively [9, 42]. The minimum *RC* of ^{40}K (0.2%) is less than the crustal abundance of 2% and the maximum of ^{40}K (3.2%) is above the crustal abundance of 2.5%. In 29 samples (97%), the *RC* of ^{238}U and ^{232}Th were all above the normal continental crust average values of 3 ppm for ^{238}U and 12 ppm for ^{232}Th, respectively. In sample S_{11}, only ^{232}Th had *RC* higher than the normal crustal average value. In 28 samples (93%), the *RC* of ^{40}K were below the crustal average value of 2.33%. Only samples S_6 and S_{24} (7%) had *RC* of ^{40}K significantly higher than the normal crustal average value of 2.33%.

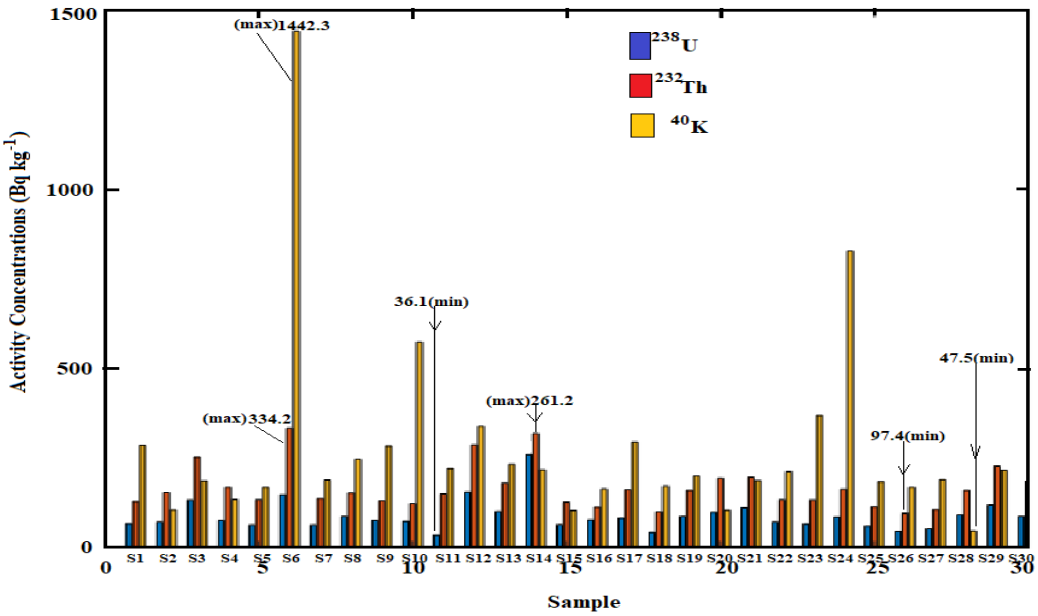

Figure 2: Bar graphs showing *AC* of ^{238}U (blue), ^{232}Th (red) and ^{40}K (yellow) in the samples.

Table 3: Comparison of average *AC* of ^{238}U, ^{232}Th and ^{40}K in the samples with those in other Countries.

Country/Study Area	Average *AC* (*Bq kg*$^{-1}$)			Reference
	^{238}U	^{232}Th	^{40}K	
Italy (Calabria Rivers)	21.3	30.3	849.0	[5]
India (Beach-Tamilnadu)	35.12	713.16	349.60	[51]
India (Cauvery River)	5.3	34.1	401.1	[40]
India (South Indian rivers)	9.81	36.49	742.46	[13]
India (Cauvery and Palar rivers)	5.31	34.04	401.11	[11]
India (Ponnaiyar river)	7.31	46.85	384.11	[25]
Egypt (Red Sea Coast)	22.2	19.2	477.6	[30]
Egypt (Aswan to El-Mania)	29.0	45.0	123.0	[16]
Egypt (Minia Nile River)	46.91	32.35	255.88	[1]
Iraq (Sulaymaniyah Rivers)	15.47	2.99	54.76	[35]
Iraq (Tigris river-Mosul City)	13.15	24.68	258.0	[9]
Iraq (Tigris River)	13.5	35.2	272.2	[28]
Iraq (Tigris River Al-Amara City)	18.22	13.79	317.34	[57]
Iran (Kerman Province hot springs)	60.78	51.43	394.37	[59]
Iran (Soleymani Hot Springs)	1630.56	39.99	125.40	[27]
Turkey (İkizdere Valley)	32.71	134.12	811.68	[8]
Bangladesh (Jamuna river)	60.0	135.0	1002.0	[55]
Russia (Potash Salts Deposit)	7.52	9.98	236.67	[58]
Algeria (Rhumel River)	26.64	25.95	165.5	[17]
Namibia (Orange River)	63.46	54.88	416.99	[56]
Nigeria (Tuomo River)	43.89	99.21	793.99	[3]
Nigeria (Imo River)	187.12	38.62	180.59	[18]
Nigeria (Osun River)	23.9	17.5	205.6	[14]
Nigeria (Yobe River)	60.0	45.0	324.0	[60]
Nigeria (llobi and Erinja Rivers)	52.0	7.6	488.0	[31]
Ghana (Tema Harbour)	34.0	30.0	320.0	[34]
Sudan (River Nile)	17.5	16.1	386.0	[37]
DR. Congo (Rivers in Mining Region)	378.0	30.0	202.0	[24]
Kenya (Bungoma County Rivers)	2.0	123.0	148.0	[32]
Kenya (Port Victoria Shoreline)	66.23	76.23	523.21	[7]
Uganda (Gulu and Amuru Rivers)	89.6	168.6	275.4	Present Study
UNSCEAR, 2000 (World limits)	35	30	400	[42]

In order to determine the existing ratio between the activity concentrations of ^{238}U, ^{232}Th and ^{40}K in the sediment samples, correlations between them were drawn using *MATLAB R*2022*b*. Figure 3 (a - c) show the correlations between the *AC* of ^{232}Th and ^{238}U, ^{40}K and ^{232}Th, and ^{40}K and ^{238}U, respectively, with a trend line drawn among the data points. In Figure 3 (a – c), linear and positive correlations were found. It can be seen that there is a good correlation between ^{232}Th and ^{238}U with correlation coefficient of (R^2 = 0.7879). The relation shows a slope of 3.689 with intercept 13.69 ppm. Similarly, Figure 3 (b) show a slope of 0.02922 with intercept of 0.1679% while Figure 3 (c) has 0.06951 and 0.5435% as slope and intercept, respectively. However, as is argued later in this paper, the most striking difference is the fact that no consistent correlations were observed between ^{40}K and ^{232}Th, and between ^{40}K and ^{238}U with weak correlation coefficients of (R^2 = 0.1841) and (R^2 = 0.05483), respectively.

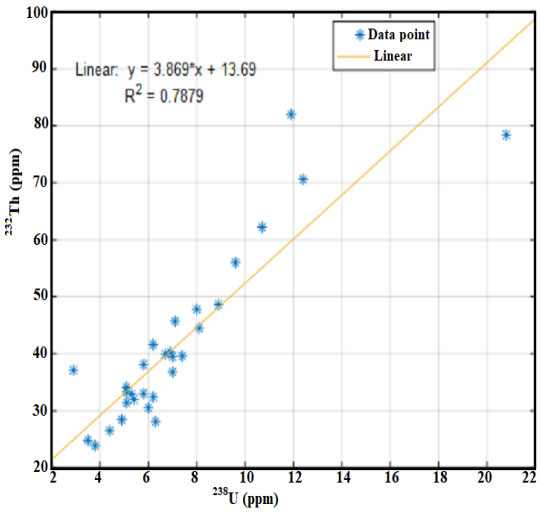

Figure 3 (a): Comparison of ^{232}Th with ^{238}U.

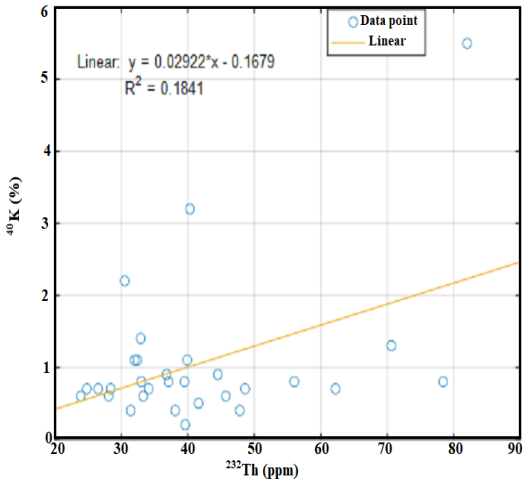

Figure **3 (b):** Comparison of ^{40}K with ^{232}Th.

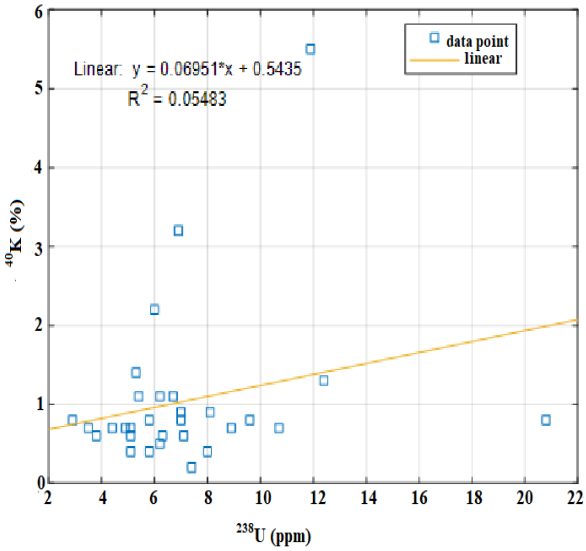

Figure 3 (c): Comparison of ^{40}K with ^{238}U.

In Table 4, the *RHP* due to the individual isotopes varied from (0.7 ± 0.06 - 5.0 ± 0.5) µW m^{-3} for ^{238}U, (1.5 ± 0.1 -5.3 ± 0.6) µW m^{-3} for ^{232}Th, and (0.006 ± 0.0004 - 0.4 ± 0.02000) µW m^{-3} for ^{40}K with averages of 1.7 ± 0.1, 2.7 ± 0.3 and 0.07 ± 0.0040 µW m^{-3}, respectively. The total *RHP* values varied from (2.5 ± 0.6 - 10.2 ± 2.6) µW m^{-3} with an average value of 4.5 ± 1.1 µW m^{-3}. The percentage contributions varied from (22.6 ± 1.1 - 49.0 ± 2.5) % for ^{238}U, (50.0 ± 2.5 - 77.4 ± 3.9) % for ^{232}Th, and (0.1 ± 0.005 - 4.7 ± 0.24) % for ^{40}K with averages of 37.8 ± 1.9%, 60.0 ± 3.0%, and 2.2 ± 0.11%, respectively. The H_f in the samples due to the decay of ^{238}U, ^{232}Th and ^{40}K varied from (19.6 ± 1.0 - 80.0 ± 4.0) mW m^{-2} with average of 35.3 ± 1.8 mW m^{-2}. Figure 4 illustrates a plot of total *RHP* and H_f producing a linear distribution segments with strong correlation coefficient of R^2 = 0.9997. The linear regression through the data points gives a slope of 7.836 km and vertical axis intercept of 0.0768 mW m^{-2}.

Table 4: *RHP* due to individual radioelements, total *RHP*, percentage contribution, and H_f ($mW\ m^{-2}$).

ID	*RHP* (U)	*RHP* (Th)	*RHP* (K)	^{238}U (%)	^{232}Th (%)	^{40}K (%)	H_f ($mW\ m^{-2}$)
S_1	1.3 (0.1)	2.1 (0.3)	0.08 (0.0050)	37.1 (1.9)	60.0 (3.0)	2.9 (0.14)	27.5 (1.4)
S_2	1.4 (0.1)	2.5 (0.3)	0.03 (0.0020)	35.9 (1.8)	64.1 (3.2)	0.8 (0.04)	31.9 (1.6)
S_3	2.6 (0.2)	4.0 (0.5)	0.05 (0.0030)	38.8 (1.9)	59.7 (3.0)	1.5 (0.08)	52.5 (2.6)
S_4	1.5 (0.1)	2.7 (0.3)	0.04 (0.0020)	35.7 (1.8)	64.3 (3.2)	1.0 (0.05)	32.9 (1.6)
S_5	1.2 (0.09)	2.1 (0.3)	0.05 (0.0030)	35.3 (1.8)	61.8 (3.1)	2.9 (0.14)	26.7 (1.3)
S_6	2.9 (0.3)	5.3 (0.6)	0.4 (0.02000)	33.7 (1.7)	61.6 (3.1)	4.7 (0.24)	67.5 (3.4)
S_7	1.2 (0.09)	2.2 (0.2)	0.05 (0.0030)	34.3 (1.7)	62.9 (3.1)	2.8 (0.14)	27.5 (1.4)
S_8	1.7 (0.1)	2.4 (0.3)	0.07 (0.0040)	40.5 (2.0)	57.1 (2.9)	2.4 (0.12)	32.9 (1.6)
S_9	1.5 (0.1)	2.1 (0.2)	0.08 (0.0050)	40.5 (2.0)	56.8 (2.8)	2.7 (0.14)	29.0 (1.5)
S_{10}	1.5 (0.1)	2.0 (0.2)	0.2 (0.01000)	42.9 (2.1)	57.1 (2.9)	0.6 (0.03)	27.5 (1.4)
S_{11}	0.7 (0.06)	2.4 (0.3)	0.01 (0.0004)	22.6 (1.1)	77.4 (3.9)	0.2 (0.01)	24.3 (1.2)
S_{12}	3.0 (0.3)	4.6 (0.6)	0.01 (0.0060)	39.5 (2.0)	60.5 (3.0)	0.1 (0.005)	59.6 (3.0)
S_{13}	2.0 (0.2)	2.9 (0.3)	0.07 (0.0040)	40.0 (2.0)	58.0 (2.9)	1.4 (0.07)	39.2 (2.0)
S_{14}	5.0 (0.5)	5.1 (0.6)	0.06 (0.0040)	49.0 (2.5)	50.0 (2.5)	0.6 (0.03)	80.0 (4.0)
S_{15}	1.2 (0.09)	2.0 (0.2)	0.03 (0.0020)	37.5 (1.9)	62.5 (3.1)	0.9 (0.05)	25.1 (1.3)
S_{16}	1.5 (0.1)	1.8 (0.1)	0.05 (0.0030)	44.1 (2.2)	52.9 (2.6)	3.0 (0.15)	26.7 (1.3)
S_{17}	1.6 (0.1)	2.6 (0.3)	0.08 (0.0050)	37.2 (1.9)	60.5 (3.0)	2.3 (0.12)	33.7 (1.7)
S_{18}	0.8 (0.06)	1.6 (0.1)	0.05 (0.0030)	32.0 (1.6)	64.0 (3.2)	4.0 (0.20)	19.6 (1.0)
S_{19}	1.7 (0.1)	2.6 (0.3)	0.06 (0.0040)	38.6 (1.9)	59.1 (3.0)	2.3 (0.12)	34.5 (1.7)
S_{20}	1.9 (0.2)	3.1 (0.4)	0.03 (0.0020)	38.0 (1.9)	62.0 (3.1)	0.6 (0.03)	39.2 (2.0)
S_{21}	2.2 (0.2)	3.1 (0.4)	0.05 (0.0030)	40.7 (2.0)	57.4 (2.9)	1.9 (0.10)	42.4 (2.1)
S_{22}	1.4 (0.1)	2.1 (0.2)	0.06 (0.0040)	38.9 (1.9)	58.3 (2.9)	2.8 (0.14)	28.2 (1.4)
S_{23}	1.3 (0.1)	2.1 (0.2)	0.1 (0.00600)	37.1 (1.9)	60.0 (3.0)	2.9 (0.15)	27.5 (1.4)
S_{24}	1.7 (0.1)	2.6 (0.3)	0.22 (0.0200)	37.8 (1.9)	57.8 (2.9)	4.4 (0.22)	35.3 (1.8)
S_{25}	1.2 (0.09)	1.8 (0.1)	0.05 (0.0030)	38.7 (1.9)	58.1 (2.9)	3.2 (0.16)	24.3 (1.2)
S_{26}	0.9 (0.07)	1.5 (0.1)	0.05 (0.0030)	36.0 (1.8)	60.0 (3.0)	4.0 (0.20)	19.6 (1.0)
S_{27}	1.1 (0.08)	1.7 (0.1)	0.05 (0.0030)	37.9 (1.9)	58.6 (2.9)	3.5 (0.18)	22.7 (1.1)
S_{28}	1.8 (0.2)	2.6 (0.3)	0.01 (0.0080)	40.9 (2.0)	59.1 (3.0)	0.3 (0.02)	34.5 (1.7)
S_{29}	2.3 (0.2)	3.6 (0.4)	0.06 (0.0040)	38.3 (1.9)	60.0 (3.0)	1.7 (0.09)	47.1 (2.4)
S_{30}	1.7 (0.1)	3.0 (0.4)	0.05 (0.0030)	35.4 (1.8)	62.5 (3.1)	2.1 (0.11)	37.6 (1.9)
Aver.	**1.7 (0.1)**	**2.7 (0.3)**	**0.07 (0.0040)**	**37.8 (1.9)**	**60.0 (3.0)**	**2.2 (0.11)**	**35.3 (1.8)**
Min.	**0.7 (0.06)**	**1.5 (0.1)**	**0.01 (0.0004)**	**22.6 (1.1)**	**50.0 (2.5)**	**0.1 (0.005)**	**19.6 (1.0)**
Max.	**5.0 (0.5)**	**5.3 (0.6)**	**0.4 (0.02000)**	**49.0 (2.5)**	**77.4 (3.9)**	**4.7 (0.24)**	**80.0 (4.0)**

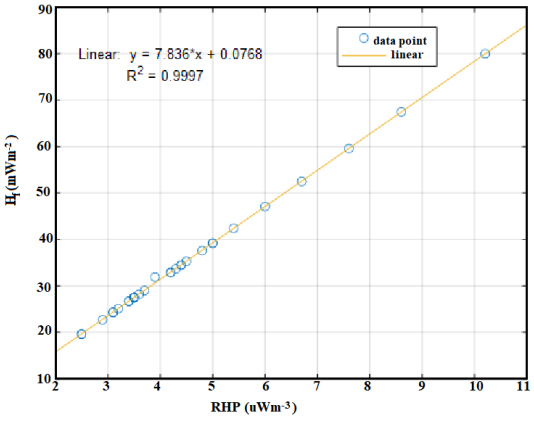

Figure 4: Comparison of *RHP* with H_f.

As can be inferred from Table 5 and Figure 5 (a), the analyzed samples were subdivided into three categories according to their *RHP*: low *RHP* samples (*RHP* < 2 µW m^{-3}), moderate *RHP* samples (2 < *RHP* < 4 µW m^{-3}) and high *RHP* samples (*RHP* > 4 µW m^{-3}) as proposed by Ethinola *and colleagues* [43] and later used by Laith

and colleagues [9] and Adagunodo *and colleagues* [44]. These assemblages show the significance of the *RHP* to the thermal regime of the region. 50% of the samples showed moderate *RHP*, another 50% showed high *RHP* and 0% showed low *RHP*.

Table 5: Classification of the studied sample in terms of *RHP*.

Low *RHP* Samples	Moderate *RHP* Samples	High *RHP* Samples
Zero samples.	S_1, S_2, S_5, S_7, S_9, S_{10}, S_{11}, S_{15}, S_{16}, S_{18}, S_{22}, S_{23}, S_{25}, S_{26}, and S_{27} (15 Samples).	S_3, S_4, S_6, S_8, S_{12}, S_{13}, S_{14}, S_{17}, S_{19}, S_{20}, S_{21}, S_{24}, S_{28}, S_{29}, and S_{30} (15 Samples).
0%	50%	50%

Figure 5 (b) illustrates the percentage contributions of ^{238}U, ^{232}Th and ^{40}K to the total *RHP*. It is very evident in Figure 5 (b) that ^{232}Th was the major contributor to total *RHP* with maximum value of 77.4%, followed by ^{238}U with maximum percentage of 49%. The ^{40}K contributed the least maximum percentage of 4.7%.

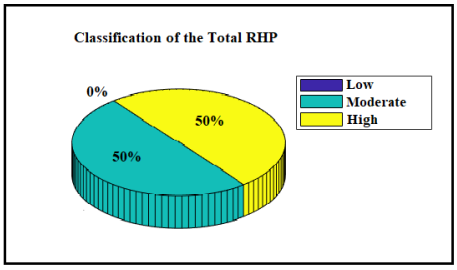

Figure 5 (a): Classification of the total *RHP*.

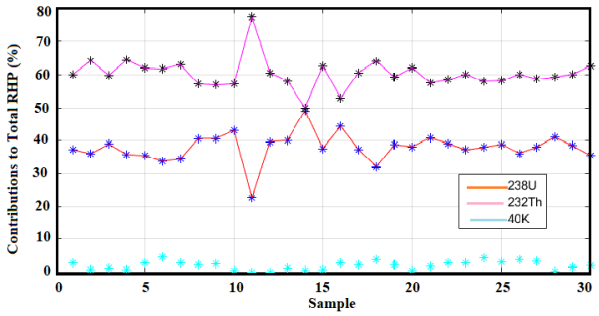

Figure 5 (b): Contributions of each isotope to total *RHP*.

4. Discussions

4.1 Activity Concentrations of ^{238}U, ^{232}Th and ^{40}K

The primeval radioactive elements ^{238}U, ^{232}Th and ^{40}K were present in all the sediment samples at varying amount. These variations may be due to the drainage pattern of the study area. It is likely that the physical and chemical (*pH*, organic content and redox) properties could have changed along the basins of the studied rivers. Similar results were also reported by the authors in [17, 24, 45] using gamma ray spectrometer techniques, who attributed them to huge variations in chemical and mineralogical properties of the provenance area. This study also found that the *AC* of ^{238}U were higher than that of ^{40}K in samples S_{14} and S_{28}. This may be due to the solubility and mobility of uranyl, $U(VI)O_2^{2+}$ in water, as has also been reported by the authors in [13, 31, 46]. Under oxidizing conditions, uranium is found in soluble *U*(*VI*) oxidation state and remains dissolved in water [12, 26, 47]. In river water, *U*(*VI*) can be reduced to insoluble *U*(*IV*) under anoxic condition and precipitate to sediments and therefore increase *AC* of ^{238}U in the sediment. This confirms the findings by the authors in [18, 24, 27, 48]. In the study by Atibu *and colleagues* [24], high *AC* of ^{238}U was attributed to artisanal mining activities while Reza *and colleagues* [27] attributed it to the existence of hot springs. Sample S_{11} had the lowest *AC* of ^{238}U of 36.1 Bq kg^{-1}, which is 1.031 times higher than the world average value of 35 Bq kg^{-1} for river sediments set by *UNSCEAR* [42]. Uranium may have become immobile under the reducing environment, due to

the insoluble nature of uraninite (UO_2) and coffinite ($USiO_4$). The sample S_{11} also showed high *AC* of ^{232}Th (151.1 Bq kg^{-1}) and low *AC* of ^{40}K (222.2 Bq kg^{-1}). Due to the high ionic potential of Th^{4+}, ^{232}Th remains in solution for a short while before being precipitated as hydroxylates or being adsorbed on clay surfaces. It is important to bear in mind, though, that, while this is true for ^{232}Th, it is not necessarily the case for ^{238}U and ^{40}K. This unique feature of ^{232}Th might have led to its significantly high *AC* in S_{11} compared to ^{238}U and ^{40}K. Recent studies by Sindani *and colleagues* [32], and Satyanarayan *and colleagues* [49] also showed *AC* of ^{232}Th greater than ^{40}K and they attributed the trend to the geological formation and type of rocks across the selected rivers. Although S_{11} showed high *AC* of ^{232}Th, it should not be forgotten that the *AC* of ^{232}Th was also higher than ^{238}U and ^{40}K in 33.3% of the samples (S_2, S_3, S_4, S_{14}, S_{15}, S_{20}, S_{21}, S_{28}, S_{29}, and S_{30}). The low *AC* of ^{40}K in the said samples was somewhat unexpected as previous studies showed that ^{40}K is the most common radionuclides with abundance of 0.012% [33]. Nevertheless, ^{232}Th has very low solubility in almost all aqueous environment. Due to the great insolubility of ThO_2 & $ThSiO_4$, ^{232}Th does not usually spread quickly through the environment when released. To a large degree, the Th^{4+} ion is insoluble, especially in acidic river sediments, and in such conditions, ^{232}Th concentration can be higher. This finding is consistent with those of Suresh Gandhi *and colleagues* [50, 51] who found that *AC* of ^{232}Th was 20.31 times higher than ^{238}U and 2.04 times higher than ^{40}K. They attributed these anomalies to the presence of the loamy sediments at Thiruvanmiyur which had relatively high amount of ^{232}Th. In contrast, sample S_{26} presented the lowest *AC* of ^{232}Th of 97.4 Bq kg^{-1}, which is 3.25 times higher than the world average of 30 Bq kg^{-1} for river sediments set by *UNSCEAR* [42]. This means that S_{26} had low amount of thorium bearing minerals. It is evident that all the analyzed samples had *AC* of ^{238}U and ^{232}Th higher than the global limits. This means that, the samples were rich in uranium and thorium bearing minerals. This undoubtedly confirms the earlier findings by Westerhof *and colleagues* [22] and Olanya *and colleagues* [33] for North Uganda terrane. This study also found that in 70% of the samples, the *AC* were in the order ^{40}K > ^{232}Th > ^{238}U, similar to the results obtained by the authors in [5, 7, 32, 52, 53]. This may be attributed to the fact that ^{40}K is the most abundant in the Earth's crust as an essential component of many light minerals. Ugbede & Akpolile [3], Abu, Abbady & Harb [6] and Elena, *and colleagues* [54] also argued in favor of ^{40}K being a naturally occurring radionuclide which abounds in the earth crust, with an abundance of 0.012% (120 ppm). Also, the *AC* in 70% of the samples show that the underlying bedrock composed of surficial materials. It was also discovered that samples S_6 (1442.3 Bq kg^{-1}), S_{10} (575.0 Bq kg^{-1}), and S_{24} (829.1 Bq kg^{-1}) had *AC* of ^{40}K higher than world average value of 400 Bq kg^{-1} by factors of 3.61, 1.44 and 2.07, respectively. This means that, S_6, S_{10}, and S_{14} had high potassium rich minerals such as feldspar, micas and clay minerals. The clayey samples were taken from rivers with weathered granitic rocks outcrops from Pogo, Coke and Kal sites, respectively. After weathering, ^{40}K could have been transported with the rock fragments by fluvial means from raised land to the sample points (S_6, S_{10}, and S_{14}) as a dissolved phase. On the contrary, 90% of the samples had *AC* of ^{40}K lower than world average value of 400 Bq kg^{-1} [42]. The primary argument in favor of the low *AC* of ^{40}K is that the 90% samples could have low content of feldspar, mica and clay minerals. A study by Sindani *and colleagues* [32] supports this observation and suggests that low *AC* of ^{40}K can be attributed to less amount of feldspar, mica and clay minerals. However, not all the analyzed samples followed this trend. In sample S_6 of Pogo site, for example, *AC* were higher than the global limits of 35, 30, and 400 Bq kg^{-1} by factors of 4.3, 11.1, and 3.6, for ^{238}U, ^{232}Th and ^{40}K, respectively. Similar high *AC* were also detected in samples S_{14} of Paminrut site, and S_{20} of Paidwe site, respectively. The samples S_6, S_{14} and S_{20} consisted of mainly fine granitic rock materials

and clay sediments. The high *AC* of the radionuclides may be due to the abundance of clay content in the studied sediments as reported by the authors in [17, 25, 47, 55, 56]. This was noted during sampling. The clay sediments, known to be a high emanator of radon, changed the water color to pale which could have increased sediment radioactivity levels. This observation is highly significant but caution is warranted as we could not scientifically link the change in water color to the detected high *AC* in the sediments. The above observation requires further investigations.

To gaze the natural radioactivity levels in the study area, the *AC* of ^{238}U, ^{232}Th and ^{40}K were compared with those in river sediments of other countries as presented in Table 3. The *AC* values in Table 3 are not the representative values for the respective countries but for the studied rivers. The values obtained in this study compare well with those reported by other authors; Ugbede [3], Masinde [7], Reza *and colleagues* [27] and Khalil *and colleagues* [55] and above the *UNSCEAR* [42] global average. Also, the *AC* values reported by the authors in [9, 14, 16, 17, 28, 32, 35, 37, 57, 58] were lower than the results presented in this paper and the global average. However, the current study found lower average *AC* of ^{238}U compared to those obtained by Ononugbo, Avwiri & Ogan [18], Atibu *and colleagues* [24], and Reza *and colleagues* [27]. Also, the average *AC* of ^{232}Th was lower than that of Suresh Gandhi *and colleagues* [51]. Furthermore, a significant discrepancy exists between the average *AC* of ^{238}U and ^{232}Th and the lower values obtained by the authors in [1, 9, 11, 16, 18, 24, 25, 30, 31, 34, 35, 37, 56, 57, 58, 59]. This discrepancy is due to the varied mineralogical and geochemical composition of parent rocks. The average of ^{40}K was lower than those reported by the authors in [3, 7, 8, 24, 55] but higher than those reported by authors in [14, 16, 17, 18, 27, 32, 35].

4.2 Radioelement Concentrations of ^{238}U, ^{232}Th and ^{40}K

The calculated average *RC* were 7.1 ± 0.5 ppm, 41.3 ± 4.3 ppm, and 1.1 ± 0.05% for ^{238}U, ^{232}Th and ^{40}K, respectively. These were above the worldwide average concentration of 2.88 ppm for ^{238}U, and 11.25 ppm for ^{232}Th but smaller than 1.31% for ^{40}K in sediments as reported by *UNSCEAR* [42] and later on cited by Laith *and colleagues* [9]. This paper reported values higher than those of Laith *and colleagues* [9] and Adagunodo *and colleagues* [44]. This shows that the studied samples had high content of ^{238}U and ^{232}Th and relatively low content of ^{40}K. This reveals the geological, geochemical and geographical conditions of the area. The values of ^{238}U and ^{40}K were lower than those found by Sabina *and colleagues* [60]. The value of ^{238}U found by Sokari *and colleagues* [36] is 1.5 times higher than the results presented in this paper. To show the relative depletion or enrichment of ^{238}U and ^{232}Th in the studied samples, the elemental concentration ratios ^{232}Th/^{238}U was determined. According to *UNSCEAR* [42], the theoretical values of the elemental ratios ^{232}Th/^{238}U are expected to be 3.0 for normal continental crust. The values obtained for the ratio ^{232}Th/^{238}U in this study varied from 3.77 - 12.80 with average of 6.09. This means there was significant fractionation of both the elements during weathering in which both uranium and thorium were enriched. These results were higher than that of the continental crust by factor of 2 and less consistent with 0.96 for Saif Eldin *and colleagues* [37], 1.9 for Faweya [61], 0.67 for Rafat [2], and 0.90 for Sathish *and colleagues* [12], respectively. The average ratio ^{232}Th/^{238}U in this study is lower than 18.99 for SureshGandhi, *and colleagues* [51], but above the world average of 3.94 reported by Sathish *and colleagues* [12]. Hence, the study area, without exception have relatively high background levels of ^{238}U and ^{232}Th from its soil (low organic content) and rock outcrops. This finding needs

further studies.

To determine the geochemical behavior of ^{238}U, ^{232}Th and ^{40}K in the studied sediments, correlation plots were done as shown by Figure 3 (a-c). The remarkable correlations between ^{232}Th and ^{238}U demonstrates that they originated from the same source, that is, the sediment samples were geochemically coherent. ^{238}U & ^{232}Th belong to actinide group of elements with similar radii (U^{4+} = 1.05 Å, Th^{4+} = 1.1 Å) and similar electron configuration (z_u = 92, z_{Th} = 90). This is consistent with the previous data reported by Khalil *and colleagues* [55], Ramadan *and colleagues* [62], and Tholkappian *and colleagues* [63], who attributed the good correlations to the likely presence of monazite minerals in the samples and that it may also demonstrate the property of the sediment samples in retaining ^{238}U, ^{232}Th and ^{40}K under varying weather conditions. Contradicting phenomenon was observed in the studies by Murugesan *and colleagues* [13], Al-Mur *and colleagues* [45], and Sylvanus *and colleagues* [56], who found weak correlations between ^{232}Th and ^{238}U of R^2 = 0.426, R^2 = 0.419, and R^2 = 0.1528, respectively. Sylvanus *and colleagues* [56] attributed this to the weak natural abundance of ^{238}U and ^{232}Th over period of times through their decay process and Murugesan *and colleagues* [13] attributed the weak correlations to minimum contribution of monazite mineral in the sample. The weak relationship between ^{238}U and ^{232}Th (R^2 = 0.451) is in general agreement with the conclusions of Uosif *and colleagues* [30] in Marine sediments of Quseir City, Egypt using NaI(Tl) detector. They attributed this to ^{238}U and ^{232}Th having some similarity in their environmental origin. The weak correlations between ^{40}K and ^{232}Th of (R^2 = 0.1841) illustrated by Figure 3 (b), shows that ^{40}K had source that was independent of ^{232}Th. During the weathering process, ^{40}K and ^{232}Th could have reacted differently. As discussed by [56], ^{40}K is more soluble and is easily carried away in water, whereas ^{232}Th tends to remain. The weak correlations between ^{40}K and ^{238}U (R^2 = 0.05483) indicated by Figure 3 (c) is probably due to the fact that ^{238}U is more soluble and mobile compared to ^{40}K. Such insignificant correlation between ^{238}U and ^{40}K (R^2 = 0.2337) and ^{232}Th and ^{40}K (R^2 = 0.0604) are conspicuous in the findings by Uosif *and colleagues* [30] and Sylvanus *and colleagues* [56], who attributed this to high potassium solubility and the anomaly in potassium existence on earth crust due to human activity. The current finding is less consistent with (R^2 = 0.853) for ^{40}K versus ^{238}U and (R^2 = 0.826) for ^{40}K versus ^{232}Th reported by Rafat [2] in sediment samples from Qarun Lake, Egypt analyzed by HPGe detector. They attributed the significant positive correlations between ^{238}U, ^{232}Th and ^{40}K to the agriculture and industrial wastes in the fine-grained sediments that were rich in organic matter content.

4.3 Radioactive Heat Production and Associated Heat Flow

To determine the geothermal potential of the study area, *RHP* of the samples were calculated. The total *RHP* values varied from 2.5 ± 0.6 - 10.2 ± 2.6 μW m^{-3} with an average value of 4.5 ± 1.1 μW m^{-3}. The average value is higher than those found by authors in [9, 11, 13, 36, 39, 40, 64, 65], but similar to those of Asere *and colleagues* [15] and Adagunodo *and colleagues* [44]. The samples were subdivided into three categories according to Ethinola *and colleagues* [43] as cited in Laith *and colleagues* [9] and Adagunodo *and colleagues* [44]. The first category shows 0% samples with low *RHP*. The second shows 50% samples with moderate *RHP*. The third shows the remaining 50% samples with high *RHP*. The most striking feature of this categorization scheme reveals that there is great heat production in the study area due to the decay of ^{238}U, ^{232}Th and ^{40}K. A common assumption is that high *RHP* in an area is associated with viable geothermal resources [9]. The

percentage contribution to the heat produced by ^{238}U, ^{232}Th and ^{40}K in the samples are summarized in Table 4 with averages of 37.8%, 60.0% and 2.2%, respectively. The ^{232}Th contributed the highest percentage to the total heat produced in the samples. The contribution of ^{232}Th to the total *RHP* was prominent in sample S_{11} of Pailyec site with the highest population of 15,042 inhabitants. As indicated in Table 4, the combined contributions of ^{232}Th and ^{238}U is 97.8% to the total *RHP*. No significant contributions to the total *RHP* came from ^{40}K, only 2.2%. The ^{238}U and ^{232}Th contributions may have come from the same source (probably from the basement rock) while that of ^{40}K may be due to mica, feldspar and clay minerals. However, the total *RHP* depicts the overall contributions from ^{238}U, ^{232}Th and ^{40}K for each sample and is a significant parameter reflecting the thermal regime of the region. This conclusion is in general agreement with the conclusions of Murugesan & Ravichandran [11], who studied sand samples from Cauvery and Palar rivers, India using NaI(Tl) detector. However, Sokari, Gbarato & Ononugbo [36] analyzed sediment samples from Okrika Local Government Area of Rivers state, Nigeria using NaI(Tl) detector and concluded that the *RHP* was mostly from ^{238}U in the order of $^{238}U > ^{232}Th > ^{40}K$. In contrast, the study by Omosule & Adelowo [38] in Osun State of Nigeria using NaI(Tl) detector discovered that ^{40}K was the major contributor to heat production compared to ^{238}U and ^{232}Th.

To determine H_f in the sampled points due to the decay of ^{238}U, ^{232}Th and ^{40}K, H_f was modeled from the values of *RHP*. The H_f in the samples varied from (19.6 ± 1.0 - 80.0 ± 4.0) mW m^{-2} with average of 35.3 ± 1.8 mW m^{-2}. This average H_f is slightly higher than 21.6 mW m^{-2} reported by Asere *and colleagues* [15] for quarry sites in Ondo State, Nigeria but less than the global value of 37 mW m^{-2} stated by Turcotte & Schubert [41] for inactive regions. Katumwehe *and colleagues* [66] reported H_f for North Uganda Terrane of between 58 - 65 mW m^{-2}, while [67] reported 34 - 70 mW m^{-2} for the Tanzanian craton. In comparison, the maximum H_f value (80 mW m^{-2}) obtained in this study maybe be an outlier, not true value for the North Uganda terrane and is beyond the scope of this work. This requires further investigation using another method. Figure 4 shows the plot of the total *RHP* against H_f with significantly strong correlation coefficient of $R^2 = 0.9997$. As expected, *RHP* in the samples produced a significantly greater effect on H_f. The H_f values reflect the high *RHP* due to decay of ^{238}U, ^{232}Th and ^{40}K in the study area, indicating feasibility for geothermal exploration. This agrees with the findings of Turcotte & Schubert [41] for stable continental areas, where the H_f had a strong correlation with the surface *RHP*. Hence, this research shows that the study area is in thermally more quiescent regions.

5. Conclusions

The average *AC* of ^{238}U, ^{232}Th and ^{40}K, and the computed *AC* of ^{238}U and ^{232}Th in all the samples were higher than the global limits. Hence, the study area is rich in uranium and thorium bearing minerals. The *AC* in 33.3% of the samples were in the order of $^{232}Th > ^{238}U > ^{40}K$, while in 70% of the samples were in the order $^{40}K > ^{232}Th > ^{238}U$. The *AC* of ^{40}K in 90% of the samples were lower than the global limits.

The samples showed 50% moderate and 50% high *RHP* with ^{232}Th contributing the highest percentage to total *RHP*. However, an increase in the concentrations of ^{238}U, ^{232}Th and ^{40}K reflected the integrated effect of *RHP*. Also, as *RHP* increases, there is observed concomitant increased in H_f. Hence the study area is suggested to have good potential for geothermal exploration and are underlain by stable continental crust.

The results of this study can be used as a baseline for further studies with special focus on the region's medium enthalpy resources such as Amoropii, Amuru and Panyimur. Particular attention should be given to parameters such as temperature, geochemistry, crustal heat flux, the origin and flow of the fluids.

6. Limitations and Recommendations

This research encountered some limitations. First, due to paucity of data on *RHP*, H_f and geothermal resources from the studied area, comparison and corroboration of previous data from the study area was difficult, though significant. To enrich the discussion and arrive at a better conclusion, the findings of this study was juxtaposed with those from other parts of the world. Therefore, this study serves as a baseline data and the basis for further research. Secondly, trace concentrations of ^{238}U, ^{232}Th and ^{40}K in the room furniture, floor, walls and possibly dust could have a significant influence on counting efficiency. This limitation was taken care of by; (i) installing the NaI(Tl) detector in the centre of the counting room, rather than around the walls to reduce background radiation from the walls, (ii) sealing the base of the detector with 15 cm wood that reduced the radiations from the floor by 20 - 25%. (iii) sealing the laboratory windows, ventilators and doors for the duration of the experiment to avoid ingress of dust. Further studies are necessary to validate the accuracy of our methods and assumptions.

Acknowledgements

The authors thank the Belgian Development Agency (*BTC* Uganda) for funding the study, Management and staff of Makerere University Physics Department for the technical support, leadership of Gulu and Amuru districts for granting permission to conduct research in the districts.

7. Conflict of Interest

The authors declare no conflicts of interest.

References

[1] S. Issa, M. Uosif, R. Elsaman. (2013, Mar.). "Gamma radioactivity measurements in Nile River sediment samples." *Turkish Journal of Engineering & Environmental Sciences*. [Online]37, pp.109 – 122. Available: https://doi.org/10.3906/muh-1207-21 [Nov. 30, 2022].

[2] M.A. Rafat. (2015, Feb.). "Radioactivity Levels in Some Sediments and Water Samples from Qarun Lake by Low–Level Gamma Spectrometry." *International Journal of Science and Research (IJSR)*. [Online] 4(2), pp. 619 – 625. Available: https://www.ijsr.net/archive/v4i2/SUB151080.pdf [Nov. 30, 2022].

[3] F.O. Ugbede, A.F. (2019, Apr.). "Akpolile, Determination of Specific Activity of ^{238}U, ^{232}Th and ^{40}K and Radiological Hazard Assessment of Tuomo River Sediments in Burutu, Delta State, Nigeria." *J. Appl. Sci. Environ. Manage.* [Online] 23(4). pp.727-733. Available:

https://dx.doi.org/10.4314/jasem.v23i4.24 [Nov. 30, 2022].

[4] R. Kritsananuwat, S. K. Sahoo, M. Fukushi, K. Pangza, S. Chanyotha. (2014, Jul.). "Radiological risk assessment of ^{238}U, ^{232}Th and ^{40}K in Thailand coastal sediments at selected areas proposed for nuclear power plant sites." *Journal of radio analytical and nuclear chemistry*. [Online] 7. pp.1-10. Available: https://doi.org/10.1007/s10967-014-3376-7 [Nov. 30, 2022].

[5] F. Caridi, M. Di Bella, G. Sabatino, G. Belmusto, M.R. Fede, D. Romano, F. Italiano, A.F. Mottese. (2021, Feb.). "Assessment of Natural Radioactivity and Radiological Risks in River Sediments from Calabria (Southern Italy)." *Appl. Sci.*[Online] 11. pp.1729. Available: https://doi.org/10.3390/app11041729 [Nov. 30, 2022].

[6] A. T. Abu, A. Abbady, S. Harb. (2019, Jan.). "Assessment of Natural Radioactivity Level in Shore Sediment Samples from Nasser Lake at Aswan, Egypt." *International Journal of Biomedical Engineering and Science (IJBES)*. [Online] 6(1). pp.1 – 11, 2019. Available: https://doi.org/10.5121/ijbes.2019.6101 [Nov. 30, 2022].

[7] T. S. Masinde. (2022, Feb.). "Radiological Impact Assessment of the Bottom Sediment Samples at Port Victoria Shoreline, Kenya." *International Journal of Applied Science and Research*. [Online] 5(1). pp. 62 – 70. Available: https://www.ijasr.org/paper/IJASR0042621.pdf [Nov. 30, 2022].

[8] R. Keser, F. G. Korkmaz, I. Alp, N.T. Okumuşoğlu. (2013, Jul.). "Determination of radioactivity levels and hazards of sediment and rock samples in İkizdere and Kaptanpaşa Valley, Turkey." *International Journal of Radiat. Research.* [Online] 11(3). pp.155-165. Available: https://www.ijrr.com/article-1-1058-en.pdf [Nov. 30, 2022].

[9] A.N. Laith, T.A. Sheamaa, Y.W. Taha, M. Howaida. (2022, Oct.). "Radiogenic heat production from natural radionuclides in sediments of the Tigris river in Mosul City, Iraq." *Int. J. Nuclear Energy Science and Technology*. [Online]15(3/4). pp. 302 – 316. Available: https://doi.org/10.1504/IJNEST.2022.126067 [Dec. 11, 2022].

[10] B. Oruru, M. Todo and A. Kisolo. (2020, Sept.). "Background Radiations and Radon Concentrations in the Dormitories of Secondary Schools in Otuke District, Uganda." *J. Rad. Nucl. Appl.* [Online] 5(3). pp. 211-218. Available: http://dx.doi.org/10.18576/jrna/050308 [Dec. 30, 2022].

[11] S. Murugesan and S. Ravichandran. (2023, Jan.). "Radioactive heat production rate and excess lifetime cancer risk of sand from two major rivers in India – A comparative study." *International Journal of Radiation Research*. [Online] 21(1). pp.117 – 124. Available: https://doi.org/10.52547/ijrr.21.1.16 [Jan. 30, 2023].

[12] V. Sathish, A. Chandrasekaran, S. Manigandan, A. Tamilarasi, V. Thangam. (2022 Feb.). "Assessment of natural radiation hazards and function of heat production rate in lake sediments of Puliyanthangal

Lake surrounding the Ranipet industrial area, Tamil Nadu." *Journal of Radioanalytical and Nuclear Chemistry*. [Online] 331. pp.1495–1505, 2022. Available: https://doi.org/10.1007/s10967-022-08207-2 [Jan. 22, 2023].

[13] S. Murugesan, S. Mullainathan, V. Ramasamy and V. Meenakshisundaram. (2016, May). "Environmental radioactivity, magnetic measurements and mineral analysis of major South Indian river sediments." *J. Mater. Environ. Sci.* [Online] 7(7). pp. 2375 – 2388. Available: https://www.researchgate.net/publication/303840881 [Nov. 30, 2022].

[14] O.A. Oyebanjo, E.O. Joshua, and N.N. Jibiri. (2012, Nov.). "Natural Radionuclides and Hazards of Sediment Samples Collected from Osun River in Southwestern Nigeria." *The Pacific Journal of Science and Technology*. [Online] 13(2). pp. 391 – 396. Available: https://www.semanticscholar.org/paper/ [Aug. 23, 2016].

[15] A.M. Asere and S.O. Sedara. (2020, Aug.). "Determination of Natural Radioactivity Concentration and Radiogenic Heat Production in Selected Quarry Sites in Ondo State, Nigeria." *NIPES Journal of Science and Technology Research*. [Online] 2(3). pp. 256 – 271. Available: https://doi.org/10.37933/nipes/2.3.2020.26 [Dec. 11, 2022].

[16] A. El-Taher & G.E. A. Adel. (2012, Apr.). "Natural Radioactivity levels and associated radiation hazards in Nile river sediments from Aswan to El-Minia, Upper Egypt." *Indian Journal of Pure & Applied Physics*. [Online] 50: 224 – 230. https://nopr.niscpr.res.in/handle/123456789/13776 [Nov. 26, 2017].

[17] B. Ghania, B. Fatima, R. Mourad. (2018, Mar.). "Levels and effects of natural radionuclides in sediment banks of Rhumel River (Northeast Algeria)." *Cumhuriyet Sci. J.* [Online] 39(2). pp. 349-356. http://dx.doi.org/10.17776/csj.360133 [Nov. 30, 2022].

[18] C.P. Ononugbo, G.O. Avwiri, C.A. Ogan. (2016, Jun.). "Natural Radioactivity Measurement and Evaluation of Radiological Hazards in Sediment of Imo River, In Rivers State, Nigeria by Gamma Ray Spectrometry." *IOSR Journal of Applied Physics (IOSR-JAP)*. [Online] 8(3). pp. 75 – 83. https://doi.org/10.9790/4861-0803017583 [Nov. 30, 2022].

[19] L. Rybach. *Determination of heat production rate: Handbook of Terrestrial Heat Flow Density Determination*. Kluwer Academic Publishers, Dordrecht, 1988, pp.125–142.

[20] S. Biira, A. W. Kisolo and F. M. D'ujanga. (2014, Nov.). "Concentration levels of radon in mines, industries and dwellings in selected areas of Tororo and Busia districts, Eastern Uganda." *Advances in Applied Science Research*. [Online] 5(6). pp.31- 44. Available: https://www.pelagiaresearchlibrary.com [May 4, 2016].

[21] M.M. Ojara., and J.P. Odongkara. "Gulu District Local Government Statistical Abstract 2012/2013."

Internet: www.unfpa.org/../170390185.pdf. Aug. 27. 2013 [May.14.2016].

[22] A.B. Westerhof., P. Härmä., E. Isabirye., E. Katto., T. Koistinen., E. Kuosmanen., T. Lehto., M. I. Lehtonen., H. Mäkitie., T. Manninen., I. Mänttäri., Y. Pekkala., J. Pokki., K. Saalmann, & P. Virransalo. "Geology and geodynamic development of Uganda with explanation of the 1:1,000,000 – scale geological map." *Geological Survey of Finland, Special Paper 55* Internet: www.gtk.fi, Jun. 23, 2014 [Apr.2, 2016].

[23] S. Adam. "Global Positioning Satellite (GPS) Visualizer. Do it yourself mapping. Portland, Oregon, USA." Internet: http://www.gpsvisualizer.com/ [Apr.15, 2017].

[24] E.K. Atibu, J.M. Oliveira, M. Malta, M. Santos, C.K. Mulaji, P.T. Mpiana, & F.P. Carvalho. (2021, Jul.). "Assessment of Natural Radioactivity in Rivers Sediment and Soil from the Copper Belt Artisanal Mining Region, Democratic Republic of the Congo." *Journal of Geoscience and Environment Protection*. [Online] 9. pp. 1-20. Available: https://doi.org/10.4236/gep.2021.97001 [Nov. 30, 2022].

[25] V. Ramasamy, G. Suresh, V. Meenakshisundaram and V. Gajendran. (2009, Oct.). "Characterization of Minerals and Naturally Occurring Radionuclides in River Sediments." *Research Journal of Applied Sciences, Engineering and Technology.* [Online]1(3). pp. 140-144. Available: https://www.researchgate.net/publication/216656959 [Nov. 26, 2017].

[26] V. Ramasamy, G. Suresh, V. Meenakshisundaram and V. Gajendran. (2009, Jan.). "Evaluation of Natural Radionuclide Content in River Sediments and Excess Lifetime Cancer Risk Due to Gamma Radioactivity." *Research Journal of Environmental and Earth* Sciences. [Online]1(1). pp. 6-10. Available: https://www.sciencedirect.com/science/article/pii/S1687850714000661 [Nov. 30, 2022].

[27] P. Reza, G. Rouhollah, R.Z. Mohamad, A. Mahdi. (2015, Feb.). "Radioactivity Concentration in Sediment and Water Samples of Hot Springs in Mahallat and Soil Samples of Their Neighboring Environs." *Environmental Studies of Persian Gulf.* [Online] 2(1). pp. 24 – 31. Available: https://www.mdpi.com/1660-4601/18/3/920 [Aug. 23, 2016].

[28] A. N. Jameel. (2022, Jan.). "Radiological Risk Assessment and Radioactivity Concentration in sediment of Tigris River of the Medical City/Bab Al Muadham." *Ibn Al Haitham Journal for Pure and Applied Science*. [Online] 3(1). pp. 28 – 38. Available: https://doi.org/10.30526/35.1.2796 [Jan. 22, 2023].

[29] M.O. Isinkaye, I.P. Farai. (2008, June.). "Activity concentrations of primordial radionuclides in sediments of surface – water dams in southwest Nigeria – a baseline survey." *Radioprotection*. [Online] 43(4). pp. 533 – 545. Available: https://doi.org/10.1051/radiopro:2008029 [Nov. 30, 2022].

[30] M. A. M. Uosif, H. Madkour, I. Shams, T. Mahmoud, and M.Z. Hesham. (2016, Jan.). "Natural

Radionuclides and Heavy Metals Concentration of Marine Sediments in Quseir City and Surrounding Areas, Red Sea Coast-Egypt." *International Journal of Advanced Science and Technology*. [Online] 86. pp. 6 – 30. Available: http://dx.doi.org/10.14257/ijast.2016.86.02 [Nov. 30, 2022].

[31] D.O. Jegede, I.A. Gbadamosi, O.O. Banjoko, J.A. Adeyoye, M.R. Gbadamosi, A.L. Ogunneye, T.E. Bakare, O.J. Oyewola. (2019, Jan.). "Radiometric and Spatial distribution of natural radionuclides concentrations and excessive lifetime cancer risks in sediments from selected rivers in llobi and Erinja communities, Southwest, Nigeria." *Nigerian Research Journal of Chemical Sciences*. [Online] 6. pp. 58 – 78. Available: http://www.unn.edu.ng/nigerian-research-journal-of-chemical-sciences/ [Jan. 22, 2023].

[32] L. Sindani, M. N. Waswa, F. Maingi and C. K. Wanyama. (2022, Feb.). "Measurement of Radiological Parameters in Harvested Sand in Bungoma County Rivers, Kenya." *Journal of Engineering and Technology for Industrial Applications*. [Online] 8(33). pp. 21-25. Available: https://doi.org/10.5935/jetia.v8i33.794 [Jan. 22, 2023].

[33] A. Olanya, D. Okello, B. Oruru and A. Kisolo. (2022, Dec.). "The Primordial Radionuclides Activity Concentrations and Associated Minerals in Rocks from Selected Quarries in Northern Uganda." *International Journal of Sciences: Basic and Applied Research (IJSBAR)*. [Online] 66(1). pp. 45-65. Available: http://gssrr.org/index.php?journal=JournalOfBasicAandApplied [Dec. 30, 2022].

[34] B.O. Botwe, A. Schirone, I. Delbono, M. Barsanti, R. Delfanti, P. Kelderman, E. Nyarko, P.N. L. Lens. (2016, Dec.). "Radioactivity concentrations and their radiological significance in sediments of the Tema Harbour (Greater Accra, Ghana)." *Journal of Radiation Research and Applied* Sciences. [Online] 30. pp. 1 – 9. Available: http://dx.doi.org/10.1016/j.jrras.2016.12.002 [Jan. 1, 2023].

[35] A. M. Hussein. (2018, Sept.). "Natural Radioactivity and Radon Exhalation in the Sediment River Used in Sulaymaniyah Governorate, Iraq, Dwellings." *The Scientific Journal of Koya University*. [Online] 6(2). pp. 7 – 12. Available: http://dx.doi.org/10.14500/aro.10381 [Jan. 22, 2023].

[36] S. A. Sokari, O. L. Gbarato and C. P. Ononugbo. (2022, Jan.). "Radiogenic Heat Production Due to Natural Radionuclides in Soil and Sediments of Coastal Communities of Okrika Local Government Area of Rivers State, Nigeria." *Asian Journal of Research and Reviews in Physics*. [Online] 6(1). pp.14-20. https://doi.org/10.9734/AJR2P/2022/v6i130174 [Jan. 20, 2023].

[37] M.B. S. Saif Eldin, A.K. Sam, A.A. O. Alfatih, S. Isam, and A.A. K. Mohammed. (2009, Nov.). "Distribution of ^{238}U, ^{232}Th, ^{40}Kand ^{137}Cs in River Nile Sediments, Khartoum, Sudan." *Phil. Nat.* [Online]1(1). pp.109 – 120. https://www.researchgate.net/publication/26619599. [Nov. 26, 2017].

[38] S. S. Omosule and A. Adelowo. (2015, Jan.). "Assessment of Radiogenic Heat Production in Soil Samples around Ife Steel Rolling Mill Site in Southwestern Nigeria." *International Journal of Innovation and Scientific Research*. [Online] 13(1). pp. 249-256. http://www.ijisr.issr-journals.org/

[Jan. 21, 2023].\

[39] A. I. C. Okeyode. (2012, Dec.). "Radiogenic Heat Production Due to Natural Radionuclides in the Sediments of Ogun River, Nigeria." *Journal of Environmental and Earth Sciences*. [Online] 2(10). pp.196 – 207. https://www.researchgate.net/publication/329454462 [Jan. 20, 2023].

[40] S. Murugesan, S. Mullainathan, V. Ramasamy, V. Meenakshisundaram. (2011, Mar.). "Radioactivity and radiation hazard assessment of Cauvery River, Tamilnadu, India." *Iran. J. Radiat. Res.* [Online] 8(4).pp. 211- 222. http://ijrr.com/article-1-683-en.pdf [Nov. 26, 2017].

[41] D.L.Turcotte and G. Schubert (1997, Jul. 13). *Geodynamics* (2nd edition). [Online]. Available: www.abebooks.co.uk/ [Mar. 5, 2023].

[42] UNSCEAR. "Sources and Effects of Ionizing Radiation." United Nations Scientific Committee on the Effects of Atomic Radiation, Report to the General Assembly, with Scientific Annexes. Sales No. E.00.IX.3, ISBN: 92-1-142238, Vol 1. New York, 2000.

[43] O.A. EThinola, E.O. Joshua, S.A. Opeloye and J.A. Ademola. (2005, Apr.). "Radiogenic Heat Production in the Cretaceous Sediments of Yola Arm of Nigeria Benue Trough: Implications for Thermal History and Hydrocarbon Generation." *Journal of Applied Sciences*. [Online] 5(4). pp. 696 – 701. Available: http://ansinet.com [Dec. 18, 2022].

[44] T.A Adagunodo, O.G. Bayowa, M.R. Usikalu, A.I. Ojoawo. (2019, Jul.). "Radiogenic heat production in the Coastal Plain Sands of Ipokia, Dahomey Basin, Nigeria." *MethodsX*. [Online] 6. pp. 1608 – 1616. https://doi.org/10.1016/j.mex.2019.07.006 [Jan. 20, 2023].

[45] B.A. Al-Mur, A. Gad. (2022, Aug.). "Radiation Hazard from Natural Radioactivity in the Marine Sediment of Jeddah Coast, Red Sea, Saudi Arabia." *J. Mar. Sci. Eng.* [Online] 10: 1145. https://www.mdpi.com/2077-1312/10/8/1145/pdf [Nov. 30, 2022].

[46] C.S Kaliprasad and Y. Narayana. (2018, Mar.). "Distribution of natural radionuclides and radon concentration in the riverine environs of Cauvery, South India." *Journal of Water and Health*. [Online] 16(3). 476 – 486. http://iwaponline.com/jwh/article-pdf/16/3/476/245976/jwh0160476.pdf [Jan. 22, 2023].

[47] V. Ramasamy, G. Suresh, R. Venkatachalapathy, V. Ponnusamy and V. Meenakshisundaram. (2010, June.). "Magnetic Susceptibility and Radiological Hazardous Nature of the River Sediments — Spectroscopical Approach." *ACTA PHYSICA POLONICA A*. [Online] 118(4). pp. 701 – 711. http://przyrbwn.icm.edu.pl/APP/PDF/118/a118z4p31.pdf [Jan. 22, 2023].

[48] J. E. Oluwagbemi and O. M. Oluwatoyin. (2016, Feb.). "Determination of Heavy Minerals and Natural Radionuclides in Beach Sediments from Badagry, Southwestern Nigeria." *Journal of Earth Sciences*

and Geotechnical Engineering. [Online] 6(2). pp.131 – 140. http://www.scienpress.com/download.asp?ID=1739 [Jun. 21, 2023].

[49] B. Satyanarayan, K. S. Sunil, S. Venkatesan, V. Balasubramanian, R. Prasanta. (2019, Jun.). "Application of multivariate technique to evaluate spatial distribution of natural radionuclides along Tamil Nadu coastline, east coast of India." *SN Applied Sciences*. [Online] 1:689. https://doi.org/10.1007/s42452-019-0716-9 [Jan. 22, 2023].

[50] M. Suresh Gandhi, R. Ravisankar, S. Sivakumar, Y. Raghu, D. A. Prem. (2013, Sep.). "Gamma-ray Spectrometric Analysis of Coastal Sediment Samples Along North East Coast of Tamilnadu." *An International Science Journal.* [Online] 4(2). pp. 21-28. https://www.researchgate.net/publication/263426764 [Aug. 23, 2016].

[51] M. Suresh Gandhi, R. Ravisankar, A. Rajalakshmi, S. Sivakumar, A. Chandrasekaran, D. Pream Anand. (2014, Oct.). "Measurements of natural gamma radiation in beach sediments of north east coast of Tamilnadu, India by gamma ray spectrometry with multivariate statistical approach." *Journal of Radiation Research and Applied Sciences*. [Online] 7: 7 – 17. http://dx.doi.org/10.1016/j.jrras.2013.11.001 [Nov. 30, 2022].

[52] E. S. Joel, M. Omeje, O. C. Olawole, G. A. Adeyemi, A. Akinpelu, Z. Embong & M. A. Saeed. (2021, Sep.). "In-situ assessment of natural terrestrial-radioactivity from Uranium-238 (^{238}U), Thorium-232 (^{232}Th) and Potassium-40 (^{40}K) in coastal urban-environment and its possible health implications." *Scientific Reports natureportfolio.* [Online] 11. pp.17555. https://doi.org/10.1038/s41598-021-96516-z [Jan. 21, 2023].

[53] A.O. Aderonke, S.O. Adeniyi, and F.A. Olarike. (2021, Aug.). "Natural radionuclides and ions concentrations in water and sediments around iron-smelting industry in Ikirun, Osun-State, Nigeria." *Journal of Public Health and Diseases*. [Online] 4(4). pp. 38 – 46. https://doi.org/10.31248/JPHD2021.103 [Nov. 30, 2022].

[54] M. Elena, P. Roman, B. Pavel, B. Sergey. (2021, Feb.). "Concentrations of Natural Radionuclides (^{40}K, ^{226}Ra, ^{232}Th) at the Potash Salts Deposit." *Journal of Ecological Engineering.* [Online] 22(3). pp. 179–187. https://doi.org/10.12911/22998993/132544 [Jan. 21, 2023].

[55] M.I. Khalil, R. K. Majumder, M.Z. Kabir, F. Deeba, M.N. Khan, M.I. Ali MI. (2016, Dec.). "Assessment of natural radioactivity levels and identification of minerals in Brahmaputra (Jamuna) river sand and sediment, Bangladesh." *Radiat Prot Environ.* [Online] 39. pp. 204-11. https://www.researchgate.net/publication/313660297 [Jan. 22, 2023].

[56] A.O. Sylvanus, N.I.K. Aina, Z. Munyaradzi, E. Emmanuel, H.H. Roswita, M.T. Bismark. (2022, Sep.). "Assessment of Radioactivity levels in shore sediments along the coastline of the Orange River, Oranjemund, Namibia." *Heliyon.* [Online] 8. pp. 1 – 7. https://doi.org/10.1016/j.heliyon.2022.e1057

[Nov. 30, 2022].

[57] H. M. A. Khalid, K. A. N. Salam, A. A. S. Zahraa. (2015, Jun.). "Natural Radionuclides and Hazards in Water and Sediment Samples of Tigris River in Al- Amara city - Maysan - Iraq." *Advances in Physics Theories and Applications*. [Online] 44. pp. 117 – 122. https://www.researchgate.net/publication/348729125 [Jan. 22, 2023].

[58] P. Mehnati, A. Jomehzadeh, V. Doostmohammadi. (2022, Jan.). "Measurement of ^{226}Ra, ^{232}Th, ^{40}K and ^{137}Cs concentrations in sediment samples and determination of annual effective dose due to these radionuclides in vicinity of hot springs in Kerman Province." *International Journal of Radiation Research*. [Online] 20(1). pp. 223-228. https://doi.org/10.52547/ijrr.20.1.34 [Nov. 30, 2022].

[59] H. T. Abba, S. Umar, D. J. Adeyemo, A. S. Aliyu, A. Ismaila, and M. A. Saleh. (2017, Dec.). "NORM distribution in coastal soils and sediments of river Yobe, North-Eastern Nigeria: An Evaluation of the Potential Radiological Hazards." *Bayero Journal of Pure and Applied Sciences*. [Online] 10(2). pp. 190 – 197. http://dx.doi.org/10.4314/bajopas.v10i2.32 [Jan. 22, 2023].

[60] Y. Sabina, S.B. Bijoy, U.K. Mayeen, K. Masud, M. R. Abdur, S.F.S. Abdul, H. Ahmed, N. Bijan, D.A. Bradley. (2018, Feb.). "The presence of radioactive materials in soil, sand and sediment samples of Potenga sea beach area, Chittagong, Bangladesh: Geological characteristics and environmental implication." *Results in Physics*. [Online] 8. pp. 1268–1274. https://doi.org/10.1016/j.rinp.2018.02.013 [Jan. 20, 2023].

[61] E.B. Faweya. (2014, Nov.). "Determination of Radioactivity Levels and Hazard of Water and Sediment Samples in Various Gold Mining Pits at Itagunmodi Ilesha Nigeria." *European Journal of Academic Essays*. [Online] 1(10). pp. 1-8. https://oaji.net/articles/2017/3667-1483553578.pdf [Nov. 30, 2022].

[62] A. B. Ramadan, M. A. Hosnia, M. T. Shadia, M. A. E. H. Thanaa, H. E. Ahmed. (2018, Apr.). "Evaluation of Natural Radioactivity and Physico-Chemical Characteristics along El-Salam Canal, Egypt." *International Journal of Engineering Science Invention (IJESI)*. [Online] 7(4). pp. 51 – 63. https://www.ijesi.org [Nov. 30, 2022].

[63] M. Tholkappian, A. Chandrasekaran, D. Ganesh, J.Chandramohan, N. Harikrishnan and R. Ravisankar. (2018, Sep.). "Determination of Radioactivity Levels and Radiation Hazards in Coastal Sediment Samples of Chennai Coast, Tamilnadu, India using Gamma Ray Spectrometry with Statistical Approach." *J. Rad. Nucl. Appl.*[Online] 3(3). pp. 171-182. http://www.naturalspublishing.com/Journals.asp [Jan. 22, 2023].

[64] A. Bubu and C. P. Ononugbo. (2018, Feb.). "Radiogenic Heat Production Due to Natural Radionuclides in the Sediments of Bonny River, Nigeria." *Journal of Scientific Research & Reports*. [Online] 17(6). pp. 1 – 9. https://doi.org/10.9734/JSRR/2017/39159 [Jan. 8, 2023].

[65] K.A. Salako, A. A. Adetona, A. A. Rafiu, U.D. Alahassan, A. Aliyu, and T. Adewumi. (2019, May). "Assessment of Geothermal Potential of Parts of Middle Benue Trough, North-East Nigeria." *Journal of the Earth and Space Physics*. [Online] 45(4). pp. 27- 42. https://doi.org/10.22059/jesphys.2019.260257.1007017 [Jan. 2, 2023].

[66] A.B. Katumwehe, M.G. Abdelsalam, E.A. Atekwana, D.A. Lao-Davila. (2015, May). "The Role of Pre-existing Precambrian Structures and Thermal Anomaly in Rift Initiation and Evolution: The Albertine and Rhino Grabens, Uganda." *Tectonophysics*. [Online] 646(1). pp. 117 – 129. http://dx.doi.org/10.1016/j.tecto.2015.01.022 [Aug. 10, 2023].

[67] S. Ballard, H.N. Pollack, and N.J. Skinner (1987). "Terrestrial heat flow in Botswana and Namibia." *Journal of Geophysical Research*. 92: pp. 6291–6300.